

Requirement for multiple activation signals by anti-inflammatory feedback in macrophages

J. Christian J. Ray, Denise E. Kirschner*

Department of Microbiology and Immunology, The University of Michigan Medical School, Ann Arbor, MI 48109-0620, USA

Received 26 July 2005; received in revised form 25 October 2005; accepted 26 November 2005

Available online 7 February 2006

Abstract

Pathogen killing is one of the primary roles of macrophages, utilizing potent effectors such as nitric oxide (NO) and involving other cellular machinery including iron regulatory apparatus. Macrophages become strongly activated upon receipt of appropriate signaling with cytokines and pathogen-derived endotoxins. However, they must resist activation in the absence of decisive signaling due to the energetic demands of activation coupled with the toxic nature of effector molecules to surrounding tissues. We have developed a mathematical model of the modular biochemical network of macrophages involved with activation, pathogen killing and iron regulation. This model requires synergistic interaction of multiple activation signals to overcome the quiescent state. To achieve a trade-off between macrophage quiescence and activation, strong activation signals are modulated via negative regulation by NO. In this way a single activation signal is insufficient for complete activation. In addition, our results suggest that iron regulation is usually controlled by activation signals. However, under conditions of partial macrophage activation, exogenous iron levels play a key role in regulating NO production. This model will be useful for evaluating macrophage control of intracellular pathogens in addition to the biochemical mechanisms examined here.

© 2005 Elsevier Ltd. All rights reserved.

Keywords: Macrophage activation; Mathematical model; Nitric oxide; Iron regulation; Biochemical network

1. Introduction

One of the primary roles of macrophages in the immune response is killing of internalized pathogens. Macrophages attain strong activation states for killing based on external signals received but must balance capability of activation with the need to stay quiescent in the absence of decisive stimuli. A resulting question is how the macrophage biochemical network balances alternate demands of different activation states. Our focus is the macrophage killing mechanism where exogenous cytokine and pathogen-derived endotoxin signals induce a genetic program resulting in the production of nitric oxide (NO) and NO-derived reactive nitrogen intermediates (Xie et al., 1992; Nathan and Shiloh, 2000) (based primarily on the well-studied mouse macrophage model). These NO-related

species have the ability to directly kill internalized pathogens (Chakravorty and Hensel, 2003) while also acting as intracellular signals (Hess et al., 2005) in feedback that regulates activation pathways (Llovera et al., 2001; Marshall et al., 2000; Marshall and Stamler, 2001) and iron homeostasis (Kim and Ponka, 2003). The link between NO and iron homeostasis can alter NO production (Weiss et al., 1994) and the availability of iron as a nutrient for pathogens (e.g. Schaible and Kaufmann, 2004). The resulting picture is of an interconnected network with systemic consequences of macrophage activation depending on the presence of activating signals and exogenous iron (Fig. 1).

Due to the energetic demands of macrophage activation coupled with the toxic and perturbative nature of nitric oxide to surrounding tissues, macrophages must remain quiescent in the absence of a decisive need for activation. When and only when the macrophage biochemical network receives a definite signal for activation, it must supply a sufficiently strong response: an integrated change in

*Corresponding author. Tel.: +1 734 647 7722; fax: +1 734 647 7723.

E-mail addresses: jjray@umich.edu (J.C.J. Ray), kirschne@umich.edu (D.E. Kirschner).

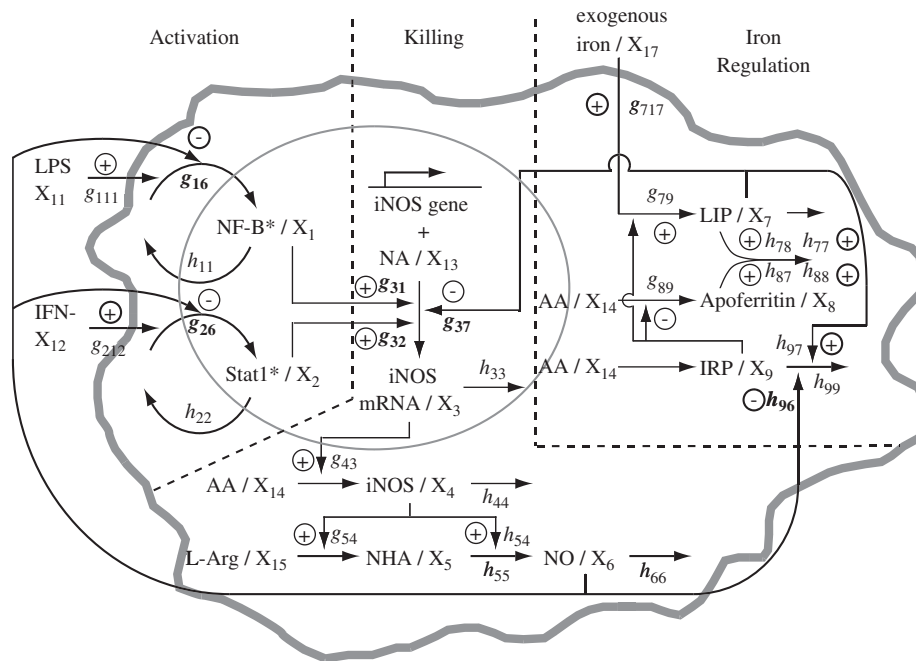


Fig. 1. Schematic of the macrophage biochemical network involved in host-pathogen interactions. Each X_i represents one model variable. Arrows pointing to or from variables represent synthetic, degradatory or cycling processes while those pointing to other arrows represent regulatory interactions. Parameters are labeled with their putative regulatory phenotype, stimulatory (+) or inhibitory (-). Three functional modules (Activation, Killing, Iron regulation) are marked. Bold parameters are subject to local detailed analysis (Methods). NA (X_{13}), pool of nucleic acid precursors to mRNA; AA (X_{14}), pool of amino acid precursors to protein. Note that the parameter h_{77} represents the weighted average of the kinetic orders from both depicted labile iron pool consumption processes.

cellular state that induces conditions leading to growth inhibition and killing of internalized pathogens. This system has a modular organizational scheme; the integrated behavior of macrophages during activation is determined by factors within and between these modules. One possibility for controlling the trade-off between quiescence and activation is based on how the functional modules interact. To address the trade-off between quiescent and activated states we have developed a mathematical model of the biochemical network operating in macrophages that reflects this organizational scheme.

Analysis of this model allows us to assess the influence of every interaction under both quiescent and activated macrophage conditions. We apply two levels of analysis here. A global statistical analysis allows us to determine the relative importance of each model parameter on macrophage activation outcomes. Local analyses of specific interactions yield network motifs that best meet evolutionary criteria for effective macrophage function. Together these analyses have revealed what network motifs allow the conflicting demands of macrophage quiescence and activation to be met. We define three functional modules of the macrophage biochemical network assessed with this approach: *activation*, *killing* and *iron regulation* (Fig. 1).

The *activation module* (AM) represents receipt of external stimuli that signal parallel second messengers: LPS-inducible NF- κ B and IFN- γ -inducible Stat1. These signals transcriptionally upregulate production of inducible

nitric oxide synthase (iNOS) (Alderton et al., 2001) in a synergistic manner (Lorsbach et al., 1993). The *killing module* (KM) represents the iNOS transcriptional program, a cascade resulting in production of NO, which serves as a signaling molecule whose products in turn regulate NF- κ B (Marshall and Stamler, 2001; Connelly et al., 2001) and Stat1 (Llovera et al., 2001) in the AM. For simplicity we emphasize NO and its effects over other killing mechanisms such as superoxide (O_2^-).

NO levels regulate amounts of iron in the labile iron pool (LIP) (Kim and Ponka, 2003), an intracellular quantity of elemental iron that is either free or loosely bound to miscellaneous weak chelators (Petrat et al., 2002) and available for metabolic use by many processes (Kakhlon and Cabantchik, 2002). LIP regulation is the primary goal of the *iron regulation module* (IRM), comprising cellular mechanisms of iron internalization and sequestration. LIP levels are increased by intake from extracellular transferrin-bound sources, and decreased by sequestration into a complex with ferritin. The IRM is coregulated with the KM via NO regulation of iron response proteins (IRPs) 1 and 2 (Hentze and Kuhn, 1996; Kim and Ponka, 2002; Wang et al., 2005) with indirect transcriptional regulation of iNOS by the LIP (Weiss et al., 1994). Thus levels of KM and IRM components are interdependent.

Our global and local analyses of the macrophage model suggest that anti-inflammatory (negative) feedback by NO from the KM to the AM allows maintenance of a system that is robust to perturbations and generally more

functionally effective than the equivalent system with no or positive feedback. This negative feedback scheme allows macrophages to stay quiescent or relatively minimally activated in the absence of decisive immune activation or under a single activation signal. However, it also allows for strong activation, but only in the presence of both endotoxin and cytokine activation signals. Only under sufficiently strong, multiple-signal activation conditions is the interaction between iNOS transcriptional regulators synergistic, a requirement for strong activation in this model. This effect partially results from NO-induced crosstalk between activation signals that suppresses one signal when the other is active. We also demonstrate that the co-regulation of NO and iron in the presence of normal iron loads is asymmetric: elevated iron levels slightly suppress NO synthesis but cytokine and endotoxin signaling more dramatically upregulates the intake and sequestration of iron. Under partial activation conditions and high iron loads the influence of these two modules on each other reaches parity; the asymmetric relationship is mostly restored under complete activation.

2. Methods

We have developed a mathematical model describing macrophage biochemical processes based on three functional modules: *activation*, *killing* and *iron regulation*. The model is built on published experimental data primarily from mouse macrophage and human cell systems. We first describe the model and then discuss the methods for how the model is analyzed. The model equations and a discussion of parameter estimation are presented in the Appendix.

2.1. Mathematical model representation

We require a representation of the macrophage biochemical network that is dynamic, accurate over a wide range of molecular concentrations and that allows analytical study. The local S-system representation of the power-law formalism (Savageau, 1996) usually meets these requirements, sometimes requiring a piecewise representation for large deviations in concentrations (Savageau, 2002). We choose this formalism over other model types due to the straightforward canonical representation of network motifs and previously developed analytical methods allowing conclusions to be drawn about the evolution of intermodule interactions.

In an S-system setting, each molecular component in the macrophage is represented by one variable described by an ordinary differential equation. An n -variable S-system is of the form $dX_i/dt = V_i^+ - V_i^-$ where each $V_i^+ = \alpha_i \prod_{j=1}^n X_j^{g_{ij}}$ and $V_i^- = \beta_i \prod_{j=1}^n X_j^{h_{ij}}$ is an aggregate power law flux describing the production and consumption of molecule X_i . Parameters α_i and β_i are rate constants for production and consumption reactions, respectively. Parameters g_{ij}

and h_{ij} are generalized kinetic orders that describe the influence of the variable X_j on the rate of X_i production or consumption (Savageau, 2001). If a variable does not influence a given flux, the kinetic order is zero. If the influence is stimulatory, the kinetic order is positive; if it is inhibitory, the kinetic order is negative. The logarithmic gain $L(x, z) = (\partial \ln x / \partial \ln z)_0$ and sensitivity $S(x, p) = (\partial \ln x / \partial \ln p)_0 = (p/x_0)(\partial x / \partial p)_0$ are useful steady state measures of the model's response where x is any dependent variable or flux, z is an independent variable, p is a kinetic order or rate constant parameter and the subscript 0 indicates values determined at steady state. Despite the formally identical definitions of gains and sensitivities, we distinguish between them because logarithmic gains represent the system's response to external signals and precursors while sensitivity refers to the consequence of small perturbations in parameters.

Our macrophage model consists of a 9-variable S-system whose mathematical specification is derived from a schematic representation of the system topology (Fig. 1). The complete set of equations is presented in the Appendix. We now highlight the representation of some key interactions; for other interactions that are relatively straightforward, we leave the details to the Appendix.

2.1.1. Activation module

We include only those variables necessary to reflect activation signaling in the context of the full model. We represent these pathways as concentrations of activated nuclear NF- κ B and Stat1. Due to the relative speed of their activation upon signaling (on the order of minutes (Nelson et al., 2002; Haspel et al., 1996) in a model that operates on the order of hours), we assume an instantaneous effect of cytokines and LPS on NF- κ B and Stat1 nuclear translocation. This is an idealized model with mechanisms of feed-forward and feedback within the AM omitted. For NF- κ B, we define the terms representing activation and feedback as $V_1^+ = \alpha_1 X_{11}^{g_{111}} X_6^{g_{16}}$ and for Stat1, $V_2^+ = \alpha_2 X_{12}^{g_{212}} X_6^{g_{26}}$ where α_1 and α_2 are rate constants, X_{11} and X_{12} are independent variables representing respective level of pathway activation from exogenous LPS and IFN- γ , and X_6 is the dependent variable [NO]. The kinetic orders g_{111} and g_{212} (both positive) scale the level of activation from respective LPS or IFN- γ signal while g_{16} and g_{26} scale NO feedback respectively (see Table 1 for specific definitions of parameters in the model). Both feedback interactions are predominantly considered negative (Llovera et al., 2001; Marshall et al., 2000; Marshall and Stamler, 2001), but not in every case for the feedback to NF- κ B, where low [NO] may have a stimulatory effect (Connelly et al., 2001). Loss of NF- κ B (Nelson et al., 2002) and Stat1 (Haspel and Darnell, 1999) activity from the nucleus due to inactivation and export are constitutive processes dependent on [NF- κ B] and [Stat1], respectively. The NF- κ B and Stat1 pathways represent parallel signals with a symmetric relationship in the model structure (Fig. 1, Activation).

Table 1
Definition and estimates of important parameters in the macrophage model

Parameter ^a	Definition	Estimated value	Sampling interval ^b
a_1	NF- κ B turnover rate (nondim)	1.73 h ⁻¹	[0.885, 41.6]
a_2	Stat1 turnover rate (nondim)	8.32 h ⁻¹	[4.62, 41.6]
a_3	iNOS mRNA turnover rate (nondim)	0.173 h ⁻¹	[0.116, 0.347]
a_4	iNOS turnover rate (nondim)	0.0693 h ⁻¹	[0.0365, 0.693]
a_5	NHA turnover rate (nondim)	5.55 μ mol/h	[0.0277, 166]
a_6	NO turnover rate (nondim)	2.77 h ⁻¹	[0.0277, 166]
a_7	LIP turnover rate (nondim)	32.20 μ mol/h	[2.58, 61.8]
a_8	apoFt turnover rate (nondim)	40 μ mol/h	[3.72, 89.2]
a_9	IRP turnover rate (nondim)	36.7 μ mol ⁻¹ h ⁻¹	[29.2, 44.1]
g_{111}	LPS-induced activation of NF- κ B	1	[0.1, 2]
g_{212}	IFN- γ -induced activation of Stat1	1	[0.1, 2]
g_{31}	NF- κ B transcriptional regulation of iNOS	1.19	[0.1, 2]
g_{16}	NO feedback to NF- κ B	-0.5	[-2, -0.1]
g_{32}	Stat1 transcriptional regulation of iNOS	0.48	[0.1, 2]
g_{26}	NO feedback to Stat1	-0.5	[-2, -0.1]
g_{37}	iron transcriptional regulation of iNOS	-0.177	[-2, -0.1]
h_{96}	NO-induced alteration of IRP	-0.5	[-2, -0.1]
g_{79}	indirect IRP-induced gain of iron influx	0.5	[0.1, 2]
g_{89}	IRP-induced translational control of ferritin	-0.645	[-1.7, -0.1]
h_{97}	iron-induced loss of IRP	0.5	[0.3, 2]

^aBoldface parameters are examined further in the local detailed analysis.

^bReduced interval sizes in g_{89} and h_{97} prevent parameter combinations that result in pathological results from the numerical solver due to stiffness in the system (see text).

This symmetry is quantitatively divided by parameter values specific to the signaling cascade.

A partial activation state is defined by receiving only one of the two activation signals. Under the partial activation state induced by treatment with LPS alone, the resultant slightly elevated [NO] may have a negative feedback effect that suppresses Stat1 activation (V_2^+) below the quiescent steady state as long as $g_{26} < 0$. Whether or not this is plausible, or if the quiescent level of Stat1 activity cannot be further suppressed, is unknown. Similarly, under activation by IFN- γ alone elevated [NO] may have a feedback effect suppressing NF- κ B activation (V_2^+) below the quiescent steady state if $g_{16} < 0$ in the model. We use a piecewise power law representation (Savageau, 2002) to prevent this suppression in a few instances to determine the effect of these assumptions (outlined in the Appendix).

2.1.2. Killing module

We represent iNOS transcriptional regulation with an mRNA production rate law: $V_3^+ = \alpha_3 X_{13}^{g_{313}} X_1^{g_{31}} X_2^{g_{32}} X_7^{g_{37}}$. NF- κ B and Stat1 regulate transcriptional initiation (Ganster et al., 2001; Gao et al., 1997) according to the kinetic orders g_{31} and g_{32} , respectively. We assume the mechanism of synergism between the activation signals here to be at the transcriptional level (Kwon et al., 2001) but it may exist earlier in the signaling cascade; see e.g. Huang et al. (2004). The LIP (X_7) regulates transcription indirectly via C/EBP- β (NF-IL6), a transcription factor required for initiation (Hentze and Kuhn, 1996; Dlska

and Weiss, 1999; Guo et al., 2003). Substituting LIP concentration into the flux term eliminates the need for representing C/EBP- β in the model. Parameter g_{37} scales the quantitative influence of the LIP on the rate of iNOS transcription initiation. We omit post-translational modification of iNOS and assume that concentrations of L-Arginine, NADPH + H⁺, and O₂ precursors to NO in iNOS catalysis are not rate-limiting (Muijsers et al., 2001). At the scale of interest here, iNOS catalyzes NO + Citrulline production via the intermediate N^ω-hydroxyarginine (NHA) (Groves and Wang, 2000). The resulting simplified pathway tracks production of NHA and NO catalyzed by iNOS (Fig. 1, Killing).

2.1.3. Iron regulation module

The IRM tracks iron response protein (IRP) regulation with a resultant influence on LIP and apoferritin levels (Fig. 1, Iron Regulation). The link between the KM and the IRM occurs through IRP regulation by NO with a resulting feedback on iNOS transcription (above). We base the network topology on the interaction between IRP2 and the cationic nitrosonium ion NO⁺ (a product that forms as a result of nitric oxide production), which presents an interaction with sufficient data for estimation of some parameters (β_9 and g_{89} from Kim and Ponka, 2002). This gives the NO control point of the IRM as the rate of IRP degradation: $V_9^- = \beta_9 X_6^{h_{96}} X_7^{h_{97}} X_9^{h_{99}}$. The majority of IRP in the cell is IRP1, which has qualitatively identical iron regulatory properties as IRP2 but possibly an opposite

response to NO (Wang et al., 2005 and references therein). To implement the assumption that either IRP1 or IRP2 is the predominant mechanism we set $h_{96} < 0$ (IRP1 or possibly IRP2) or $h_{96} > 0$ (IRP2). We assume IRP-regulated transcript stabilization of the transferrin receptor and resultant increase in iron influx (reviewed in Thomson et al., 1999) is directly controlled by IRPs. This is included in the iron influx term V_7^+ . Lastly, IRPs translationally control apoferritin production (Thomson et al., 1999). Apoferritin subunits form a shell structure that holds the sequestered iron atoms within. The ratio of iron atoms to ferritin protein complexes is about 4000:1 in the iron-rich ferritin complex (see Theil, 2003 for a short review). Iron accumulates in the ferritin complex relatively slowly, continuing for up to 24 hours after initial iron loading (Herynek et al., 2000). Based on the rate of this process, we assume that the variable X_8 represents the molarity of binding capacity held by ferritin rather than the raw number of molecules. The iron-rich ferritin complex is stored by macrophages for use by other cells, maturing into hemosiderin under conditions of iron overload (Harrison and Arosio, 1996). The primary source of LIP is presumably transferrin-bound extracellular iron. Low extracellular iron results in degradation of the ferritin complex to replenish the LIP in red blood cells (Konijn et al., 1999). Since we do not simulate low iron conditions, and since the iron-rich ferritin complex is stored for long periods by macrophages, the fate of this complex is beyond the scope of the model.

2.2. Parameter estimates

Our goal is to derive order-of-magnitude estimates for model parameters resulting in behavior that reflects the known data for the physical macrophage system. Uncertainty and sensitivity analyses can then be used to explore the parameter space and determine variations in system outcome. The macrophage model contains 44 parameters whose values require estimation before numerical model simulations can be performed. Complete details of this process are given in the Appendix and summarized in Table 1. Here we outline some key steps.

First, we reduce the number of estimates needed using non-dimensionalization. The non-dimensionalized model is used for numerical simulations, but we use the dimensionalized model for calculation of stability and robustness, which do not require numerical simulations (see local analysis, below). Non-dimensionalization of the model gives a normalized form with concentrations relative to the quiescent steady state; the effect of kinetic orders across the two model forms is the same.

Substituting levels of each variable X_i relative to quiescent steady state \hat{X}_i gives the non-dimensional value $x_i = X_i/\hat{X}_i$ (we use the \hat{y} notation to distinguish the particular quiescent steady state of y from the generic steady state denoted by y_0). In this type of model, a unique steady state always exists as long as the determinant of the

matrix \mathbf{A} of kinetic order differences is non-zero (i.e. $\det \mathbf{A} = \det[g_{ij} - h_{ij}] \neq 0$; see Voit, 2000, pp. 200–201). At the steady state, $\alpha_i \prod_{j=1}^{n+m} X_{j0}^{g_{ij} - \delta_{ij}} = \beta_i \prod_{j=1}^{n+m} X_{j0}^{h_{ij} - \delta_{ij}} = a_i$ where $\delta_{ij} = \begin{cases} 1, & i=j \\ 0, & i \neq j \end{cases}$ and m is the number of independent variables (six here). Then $\hat{x}_i = 1$ for $i = 1, \dots, 9$ represents the quiescent steady state in the non-dimensionalized model. Table 1 gives estimated values for turnover rates and kinetic orders for most of the parameters. Several kinetic order parameters are omitted from Table 1 as they are set to the value 1 (see Appendix for details).

2.3. Software and simulations

We used two platforms to perform simulations to ensure that convergence to the same solutions occurs in different settings. Mathematica (Wolfram Research) was used for most calculations. The results were confirmed with a second program written by our group in C++ incorporating standard ODE solvers. An algorithm for uncertainty and sensitivity analysis was implemented in both and the results compared for accuracy. Steady state analysis, including dose-response and calculation of logarithmic gains and sensitivities were done using Mathematica's algebraic Solve function.

2.4. Global statistical analysis

Estimating parameters for any mathematical model is complicated by lack of or variability in experimental data. This leads to uncertainty in the quantities used for parameters. We have implemented statistical uncertainty and sensitivity analyses (Helton and Davis, 2000) that allow simultaneous exploration of the entire biologically plausible parameter space.

We used a type of stratified Monte Carlo sampling known as Latin Hypercube Sampling (LHS) to partition wide parameter ranges into a number, N , of equiprobable subintervals for high efficiency sampling (McKay et al., 1979; Blower and Dowlatabadi, 1994). This method prescribes sampling once per subinterval. Therefore, the greater the partition number N , the more accurate the estimates of sensitivity will be. We chose a partition number of $N = 1000$ and randomly combined the sampled numerical values, one value per parameter. In the absence of further data on their actual distributions, each parameter interval was sampled assuming a uniform distribution for the ranges specified in Table 1. The intervals chosen for the kinetic order parameters represent a sampling of the parameter within a region corresponding to one type of regulation; i.e. always positive or negative. Distinguishing between the qualitative differences in regulatory motifs (positive, negative or no regulation) is left to the local analysis discussed below. Note that the intervals for two parameters (g_{89} and h_{97}) were slightly reduced to avoid numerical stiffness resulting from x_8 ([apoferritin]/[apoferritin]₀) becoming too small during simulation.

We perform simulations of the system for a 100-hour time frame after a constant stimulus of LPS, IFN- γ , and/or exogenous iron starting from quiescent steady state conditions. This analysis uses the non-dimensionalized model for numerical simulations. Due to the non-dimensionalization, the quiescent steady state concentration of each molecule in the model is 1. Statistical measures describe the output with a lognormal distribution when the system is near steady state. Here, the output is the distribution of values for the dependent variable x_6 representing $[\text{NO}]/[\text{NO}]_0$. Our goal in choosing the treatment levels (which are arbitrary) is to induce distinct *activation states* above this steady state given by particular levels of exogenous LPS, IFN- γ and iron (x_{11} , x_{12} and x_{17} , respectively).

Stimulation of the AM from LPS or IFN- γ is set to 100-fold induction of NF- κ B or Stat1, respectively. This quantity is chosen to represent a level of activation that is definite and distinguishable from an insignificant stimulus but well below high activation levels that cause signal saturation. Therefore, $x_{11} = 100$ and $x_{12} = 100$ under conditions of complete activation. Under partial activation conditions, either NF- κ B or Stat1 is subject to 100-fold activation, but not both. The quiescent level of activation is given by $x_{11} = 1$, $x_{12} = 1$.

Under iron-rich conditions, the intake of exogenous iron into the LIP is increased 10-fold (over low iron conditions of $x_{17} = 1$); that is, $x_{17} = 10$. This simulates conditions of high iron levels and their effects on overall macrophage activation. There is a constant background level of the LIP that is measurable under homeostatic conditions (see for example Petrat et al., 2002). Therefore, in contrast to the second messengers in the model, a relatively small fold-change in iron intake will simulate iron-rich conditions.

When performing the LHS analysis described above, we are able to measure uncertainty in the outcome variable (x_6 : $[\text{NO}]/[\text{NO}]_0$) due to changes in the parameter values. What remains to do is to correlate the observed variations to specific parameters. This can be accomplished using a partial rank correlation (PRC) (see Blower and Dowlatabadi, 1994) as a *statistical sensitivity*. The resulting correlation coefficients, γ_{iy} , have a magnitude between 0 and 1, and a sign (+/−) describing the relationship of the i th input parameter to the y th variable. The PRC may be calculated at any time point during the simulation; many of the correlations are dynamic. A significance test has been determined for γ_{iy} (versus $\gamma_{iy} = 0$) that approximates a Student's T (Blower and Dowlatabadi, 1994). The PRC is valid when considering solutions with a monotonic relationship with respect to the input parameter (Helton and Davis, 2000) as is the case here. We have also implemented a Z test for comparisons of PRC coefficients against one another to determine the relative statistical sensitivity of variables to different parameters in a particular activation state (Howell, 1987, pp. 240–241). We refer to the magnitude of the PRC without regard to sign as the *absolute PRC*.

2.5. Local detailed analysis

To evaluate the role of specific parameters within the macrophage biochemical model, we apply a local detailed analysis. We view the macrophage as a modular system where signals from a given module co-regulate other modules resulting in a new cellular state. Thus, parameters governing the interaction of the three functional modules are of particular interest toward understanding the trade-off between macrophage quiescence and activation.

In this setting we apply mathematically controlled comparisons (MCCs) that allow evaluation of the inter-module parameters and their influence on model outcomes according to a set of *Criteria for Functional Effectiveness* (CFE) (Irvine, 1991). This method is analogous to a gene knockout experiment where part or all of a specific pathway is deleted from a system. In our case, a component of the pathway (e.g. gene product) is not deleted but one effect of the component on another member of the pathway is neutralized, increased, decreased or reversed. We refer to the interaction under study this way as a “knockout” parameter. The knockout system is compared to the wild-type (control using the default parameter values in Table 1, column 3) based on their conformity to the CFE. The CFE used to assess changes in functional effectiveness as a parameter varies are three well-defined criteria that have been applied to study other inducible systems (Hlavacek and Savageau, 1995). The first, *stability*, is the ability of the system to return to steady state after a transient perturbation as evaluated by the last Routh–Hurwitz criterion (outlined in Voit, 2000, pp. 208–213; for this model given in Table 3). Second, *robustness*, is insensitivity of dependent variables and fluxes to perturbation by independent variables and parameters; this is measured by steady state logarithmic gains and sensitivities. Lastly, *responsiveness* is the minimal time for $[\text{NO}]/[\text{NO}]_0$ (x_6) to reach a new steady state from the quiescent steady state after a stimulus. Induction of NO under a decisive signal is also a requirement for a functionally effective system, but this will be indirectly required for all parameter values tested to meet an equivalence requirement as part of the MCC (below) and thus need not be an explicit criterion. Each of the six knockout parameters that we explored in local analysis are listed in Table 2 columns 1–2.

Mathematically, stability and robustness can be determined from the system at steady state making no specific choices for parameter values (using the dimensionalized model). This lends generality to the results. For the stability and robustness criteria, we were able to perform the analysis in the most general setting, making no assumptions on the numerical values for the parameters. The results are often shown with default parameter values (Table 1) substituted for simplicity of presentation. Unlike stability and robustness, the responsiveness criterion requires numerical simulations with specific values for each parameter using the non-dimensional model.

Table 2
Parameters examined in the local detailed analysis

Parameter ^a	Function	Corrected parameters	Constrained parameter space
g_{31}	NF-κB transcription	$g_{32}; g_{37}; g_{313}; \alpha_3$	$g_{31} \times g_{37}$
g_{32}	Stat1 transcription	$g_{31}; g_{37}; g_{313}; \alpha_3$	$g_{32} \times g_{37}$
g_{16}	NO feedback to NF-κB	$g_{111}; \alpha_1$	$g_{16} \times g_{111}$
g_{26}	NO feedback to Stat1	$g_{212}; \alpha_2$	$g_{26} \times g_{212}$
g_{37}	Iron control of transcription	$g_{31}; g_{32}; g_{313}; \alpha_3$	$g_{37} \times g_{31}$
h_{96}	NO control of iron regulation	$h_{97}; h_{99}; \beta_9$	$h_{96} \times h_{97}$

^aShown for each parameter is its definition, a set of other parameters in the same flux term corrected to ensure external equivalence requirements in each case, and a constrained parameter space used for its line of equivalent gain that ensures a controlled comparison (see Methods).

Table 3
Lines of equivalent gain and the stability criterion used for local detailed analysis

Parameter(s)	Line of equivalent gain
g_{31}, g_{32}	$g_{37} = \frac{(p_1+p_2+L_s(p_3+p_4-p_5))(p_7h_{97}-p_8)}{g_{43}g_{54}h_{11}h_{22}h_{96}L_s p_7}$
g_{37}	$g_{31} = \frac{-p_2(p_7h_{97}-p_8)+L_s(p_6p_7+(-p_4+p_5)(p_7h_{97}-p_8))}{g_{43}h_{22}(g_{111}h_{66}+g_{16}g_{54}L_s)(p_7h_{97}-p_8)}$
g_{16}	$g_{111} = \frac{-p_2(p_7h_{97}-p_8)+L_s(p_6p_7-(p_3+p_4-p_5)(p_7h_{97}-p_8))}{g_{31}g_{43}h_{22}h_{66}(p_7h_{97}-p_8)}$
g_{26}	$g_{212} = \frac{-p_1(p_7h_{97}-p_8)+L_s(p_6p_7-(p_3+p_4-p_5)(p_7h_{97}-p_8))}{g_{32}g_{43}h_{11}h_{66}(p_7h_{97}-p_8)}$
h_{96}	$h_{97} = \frac{p_1p_8+p_2p_8+L_s(p_6p_7+(p_3+p_4-p_5)p_8)}{(p_1+p_2+L_s(p_3+p_4-p_5))p_7}$

Stability criterion

$$p_6p_7 - (p_3 + p_4 - p_5)(h_{97}p_7 - p_8) > 0$$

Abbreviation	Value	Abbreviation	Value
p_1	$g_{111} g_{31} g_{43} h_{22} h_{66}$	p_5	$h_{11} h_{22} h_{33} h_{44} h_{66}$
p_2	$g_{212} g_{32} g_{43} h_{11} h_{66}$	p_6	$g_{37} g_{43} g_{54} h_{11} h_{22} h_{96}$
p_3	$g_{16} g_{31} g_{43} g_{54} h_{22}$	p_7	$g_{89} h_{78} - g_{79} h_{88}$
p_4	$g_{26} g_{32} g_{43} g_{54} h_{11}$	p_8	$(-h_{78}h_{87} + h_{77}h_{88})h_{99}$

As part of the MCC, we force the value of a knockout parameter to change. To control for changes as this parameter is varied, we require the model to maintain equivalence with the wild-type (default parameter value) case over the parameter range in two ways: internally and externally (Savageau, 2001). *Internal equivalence* requires that the parameters not associated with the flux containing the knockout parameter under study remain the same. *External equivalence* requires the external behavior of the model to remain the same as the parameter under study is varied; this then requires correction of other parameter values in the same flux as the knockout parameter. In each case we use iNOS induction to measure external behavior. iNOS levels are a direct readout of gene expression, reflecting equivalence in the macrophage gene expression program across values of the knockout parameter. (We could as easily use NO as the external measure of behavior, with the process almost identical and the conclusions unchanged.) At wild-type iNOS levels for a given activation stimulus, we must adjust the other parameters in the flux containing the knockout parameter under study. Two requirements for iNOS levels must be met: as the knockout parameter is varied, the model must have an identical quiescent steady state (\bar{X}_4) and identical

total logarithmic gain ($L_s = L(X_4, X_{11}) + L(X_4, X_{12}) + L(X_4, X_{17})$) with respect to exogenous signals that influence the macrophage activation state (LPS, IFN-γ, and extracellular iron levels). Table 2, column 3, shows which parameters require adjustment to meet the external equivalence requirement. The number of parameters requiring correction in the flux determine the degrees of freedom for the interaction of interest. The corrected parameters are both kinetic orders and rate constants. In the non-dimensionalized system (used for numerical simulations) finding the equivalence for rate constants is unnecessary because the normalized quiescent steady state is the same for any chosen value of the parameter of interest. Thus we only correct the kinetic orders in this case, and find a *line of equivalent gain* (LEG) over the range of the parameter under study that gives the parameter corrections for external equivalence. Note that the computation of stability is also independent of rate constants (Table 3, Stability criterion) leaving only the robustness criterion requiring correction of rate constants during the comparison.

In the examination of the robustness criterion for various g_{31} , g_{32} and g_{37} , we also require correction of g_{313} by holding $L(X_4, X_{13})$ constant, allowing the unbiased

determination of systemic sensitivities. This correction is not required for the other criteria: stability is independent of g_{313} and the non-dimensional model is identical for changes in this parameter because levels of precursors are assumed not to be perturbed during the calculation of responsiveness.

As an example of the MCC method, we outline the procedure for g_{16} , which represents the feedback of nitric oxide (X_6) in the KM to the activating second messenger NF- κ B (X_1) in the AM (Fig. 1). We require $L_s = L(X_4, X_{11}) + L(X_4, X_{12}) + L(X_4, X_{17})$ for every g_{16} quantity investigated. From this relationship we find the correction factor for parameters in the same flux term as the knockout parameter examined, in this case g_{111} . This corrects g_{111} so that:

$$g_{111} = \frac{-p_2(p_7 h_{97} - p_8) + L_s(p_6 p_7 - (p_3 + p_4 - p_5)(p_7 h_{97} - p_8))}{g_{31} g_{43} h_{22} h_{66} (p_7 h_{97} - p_8)}$$

(Table 3). This is the LEG for the NO feedback parameter g_{16} , ensuring external equivalence in the model for the MCC.

Clearly, alteration of L_s can change the slope of the LEG, and possibly change results for very large changes in L_s . Here we restrict L_s to approximate what is experimentally found in mouse macrophage cell culture (see Parameter estimation above). In principle, representation of this network in other cell types or species with much lower or higher L_s may require adjustment of the slope of the LEG.

We visualize three possible regions in a parameter space with the knockout parameter of interest on the x -axis and the parameter corrected to ensure external equivalence on the y -axis (for example, Fig. 6B for g_{16}). Each point on the LEG represents one set of parameters for model evaluation according to the CFE. Note that g_{16} has one degree of freedom, giving a two-dimensional parameter space. The distance d on the LEG represents the distance between a stable parameter value choice and the line generated from the stability criterion, allowing the determination of stability by d . Robustness and responsiveness of the system represented by a given point on the LEG are determined with the calculations or simulations specified by the definition of the CFE above.

We have found the LEG for parameter g_{16} as an example of applying MCC to one of the six interactions between the functional modules. Certain considerations are necessary to generalize the process to the other five knockout parameters (Table 2). Applying MCC for the KM feedback to Stat1 (g_{26}) follows directly from the above process. However, an additional degree of freedom is found for the other MCCs due to the higher number of components regulating the processes. For instance, parameters g_{31} , g_{32} and g_{37} each require correction of either of the other two parameters for equivalence (Table 2), leading to a plane of equivalent iNOS logarithmic gain in three-dimensional parameter space. For simplicity we choose to reduce the

degrees of freedom in these cases by holding one parameter constant and meeting the equivalent gain requirement by correcting the other (2). The parameter held constant is given the default wild-type value in Table 1. In this way all of the MCCs are performed in the constrained parameter space given in Table 2.

For each of the six parameters we evaluated using the CFE (Table 2), we assign a *score* for each criterion of + (stimulation of a process), - (inhibition of a process) or 0 (no regulation of a given process). Then the overall score is calculated based on the individual score for each criterion. The overall score represents the type of regulation that is assigned as *optimally functionally effective* for a given interaction. Recall each knockout parameter represents the regulation of a rate of production or consumption of a molecular component of the model. Thus the overall CFE score for a parameter predicts the type of regulation that optimizes the overall macrophage performance.

3. Results

Macrophages require maintenance of a quiescent state to conserve energy and minimize host damage while oppositely needing to be sufficiently activated under appropriate conditions to best control or kill pathogens. Our aim is to understand and predict necessary requirements for the trade-off between these macrophage states. To this end, we have developed a mathematical model representing the biochemical network operating within macrophages that is based on a framework of functional modules. Here we present results from our analyses of the model in three parts: validation simulations, global uncertainty and statistical sensitivity analysis, and a local analysis of functional effectiveness based on three specified criteria.

3.1. Conditional synergistic activation by two signals

To validate the model system, we compared the model's predicted steady state dose-response [NO] with simulated LPS and IFN- γ doses to data from macrophage cell culture (Fig. 2). With only quiescent levels of LPS-induced NF- κ B stimulation even a significant increase in IFN- γ -induced Stat1 levels leads to very low NO induction above [NO]₀. Results with increasing amounts of LPS and IFN- γ stimulation show a capacity for synergistic induction of iNOS and resultant NO production (Fig. 2A). This has been previously observed in experiments using sub-saturation levels of LPS and IFN- γ measuring nitrite output of J774.1 macrophage cell cultures (Fig. 2B). In the model, the mechanism behind this phenomenon arises from the flux term V_3^+ (iNOS transcriptional regulation) from the interactions of NF- κ B and Stat1.

The model predicts a dual role for transcriptional activation parameters, exhibiting either a synergistic or

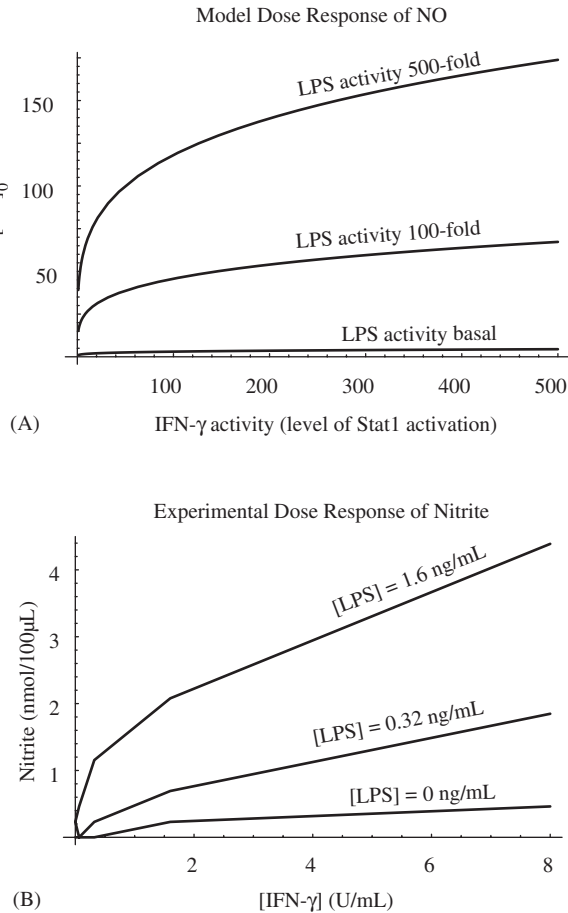


Fig. 2. (A) Steady state dose response of NO (x_6) in the macrophage model for various levels of NF- κ B and Stat1 induction by LPS (x_{11}) and IFN- γ (x_{12}), respectively, shows synergistic activation by multiple activation signals. (B) Dose response of nitrite to various concentrations of LPS and IFN- γ in J774A.1 mouse macrophages shows a similar synergistic activation. Data are from Chauhan et al. (2004); we selected a subset of the data that is below saturation.

non-synergistic influence on transcriptional activation (Fig. 3, $g_{16}, g_{26} < 0$). Under dosing of only one activator (for example, LPS) low-dose levels of IFN- γ (less than \ddagger in Fig. 3B) do not allow a synergistic influence of NF- κ B and Stat1 interactions on transcription, while higher levels of IFN- γ alter the sensitivity of NO to transcriptional activation such that the interaction of NF- κ B and Stat1 is synergistic. The model mechanism causing this phenomenon is negative feedback on Stat1 by NO, induced from the LPS/NF- κ B-activation pathway. This feedback induces the IFN- γ /Stat1 pathway to be at or below its quiescent steady state level.

This crosstalk is confirmed by comparing the sensitivity $S(x_6, g_{32})$ when varying the feedback parameter g_{26} (Fig. 3B). The non-synergistic activation state is abolished in the absence of this feedback ($g_{26} = 0$) or when it is positive ($g_{26} > 0$). We thus find that negative feedback crosstalk (that is, feedback on Stat1 under primarily LPS signaling or feedback on NF- κ B under primarily IFN- γ

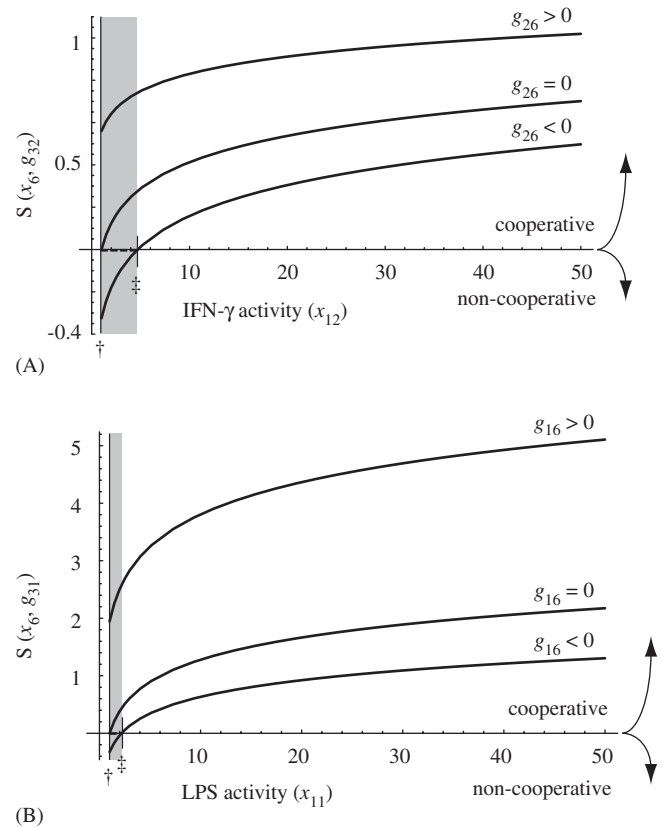


Fig. 3. Crosstalk of activation pathways induced by common feedback. (A) The sensitivity of [NO] to alterations in Stat1 transcriptional effect (g_{32}) under constant LPS activity ($x_{11} = 100$) shows a dependence on IFN- γ activity (x_{12}). During activation from LPS but low IFN- γ signaling, the negative feedback by NO to Stat1 can cause it to have a non-cooperative influence on iNOS transcriptional activation (gray shaded region). Above a certain threshold of IFN- γ -induced Stat1 activation (marked \ddagger) the interaction is cooperative, or synergistic ($S(x_6, g_{32}) > 0$). (B) Sensitivity of [NO] to alterations in NF- κ B transcriptional effect (g_{31}) under constant IFN- γ activity ($x_{12} = 100$) shows a parallel effect. This effect in both cases is altered under cases lacking feedback ($g_{26}, g_{16} = 0$, respectively) or with positive feedback ($g_{26}, g_{16} > 0$, respectively) where the sensitivity measure does not reach zero above the quiescent steady state (marked \dagger). The dashed lines (between \dagger and \ddagger on the x -axis) represent S for negative feedback when a piecewise model is used to prevent suppression of the activation module below the quiescent steady state (see text for explanation). Values of g_{16} and g_{26} are chosen with the constraints of lines of equivalent gain described in Methods.

signaling) contributes to maintenance of a quiescent macrophage state in the absence of multiple decisive activation signals. The possibility of low [NO] having a positive feedback effect for NF- κ B (Connelly et al., 2001) brings this effect into question under conditions of partial activation with high IFN- γ signaling but low LPS signal (Fig. 3A). If the level of NO induced by IFN- γ alone is high enough to surpass this proposed low-level positive feedback threshold then the effect can occur (and indeed is predicted by the model). Note that for optimal maintenance of quiescence we predict negative feedback ($g_{16} < 0$) for this low-level activation (discussed below).

3.2. Global analysis: statistical sensitivities of parameters under different activation stimuli and exogenous iron treatments

To determine global statistical sensitivity of chosen model outputs with respect to changes in parameter values from Table 1, we applied uncertainty and statistical sensitivity analyses using LHS and PRC, respectively, with a sampling partition of $N = 1000$ as described in methods. With the non-dimensionalized model form used for this part of the analysis, references to concentrations of components (e.g. [NO]) refer to the normalized concentration. This analysis was performed under six different activation signaling states: LPS alone, IFN- γ alone, LPS + IFN- γ and each of the above together with exogenous iron. We find PRCs for [NO] (x_6) at a time point of $t = 100$ h after initial stimulation, which is at (or near) the steady state for the 1000 simulations. The results are summarized in Figs. 4 and 5. In Fig. 4, Panel A indicates sensitivities of [NO] to parameters on the interface of the AM and KM, while Panel B indicates sensitivities of LIP level to these parameters. In Fig. 5, Panel A indicates PRC coefficients in the absence of exogenous iron and Panel B indicates PRC coefficients in the presence of exogenous iron for parameters in the IRM, including those on the interface of the KM and IRM.

Because we performed the analysis with [NO] near the activated steady state, we find that turnover rates (a_i) do not have a significant influence on outcome variable (NO/ x_6 or LIP/ x_7) levels. Carrying out a statistical sensitivity analysis under pre-steady state conditions revealed that some turnover rates have significant but minor PRCs: $\gamma_{a_i, x_i} < \pm 0.25$. This is almost always the case for iNOS mRNA and protein turnover rates a_3 and a_4 and in some cases NO and LIP turnover rates a_6 and a_7 as well. As component levels change over time after stimulation, the kinetic order PRCs (γ_{g_{ij}, x_i} and γ_{h_{ij}, x_i}) change in a predictable manner: those related to the AM and KM generally follow [NO] while those related to the IRM

generally follow [LIP]. These transient PRCs are in line with intuition, but in this work we emphasize steady state correlations due to our focus on distinct activation states.

Under the various stimuli, one obvious result is that kinetic order parameters have a much stronger PRC with [NO] when their corresponding pathway is activated than when it is not activated. For example, g_{111} , the kinetic order characterizing the change of NF- κ B activation levels with LPS treatment (Fig. 4) has a high PRC under stimuli that include LPS but not during treatment with IFN- γ alone, with or without exogenous iron. As we would expect, most parameters involved in either the AM or KM (Fig. 4) have stronger absolute PRCs with [NO] than those of the IRM (Fig. 5).

3.2.1. Interactions between the activation and killing modules

The interaction between the AM and KM is determined by parameters representing transcriptional activation (g_{31}, g_{32}) and feedback by NO (g_{16}, g_{26}). We find the PRCs to be primarily dependent on the activation state with regard to LPS and IFN- γ but only slightly on the level of exogenous iron (Fig. 4). For each activation state we assume that NF- κ B and Stat1 can be regulated both up and slightly down. If we assume that the AM cannot be downregulated below the quiescent state (see the piecewise model variant in Methods and Appendix) some PRCs become non-significant (Fig. 4 \dagger).

Under both model variants NO crosstalk contributes to maintenance of quiescence. Under signaling conditions biased strongly to one signal or the other (i.e. LPS or IFN- γ alone) we find the PRCs for the two transcriptional activation parameters (g_{31} and g_{32}) to have opposite signs (+ in one, – in the other) while the statistical sensitivity of [NO] to KM feedback to the AM is negative. Recall that $g_{16}, g_{26} < 0$ here; thus, a positive PRC means a negative correlation between strength of feedback and [NO] (Fig. 4). This effect is abolished under full activation: both transcriptional activation parameters have positive correla-

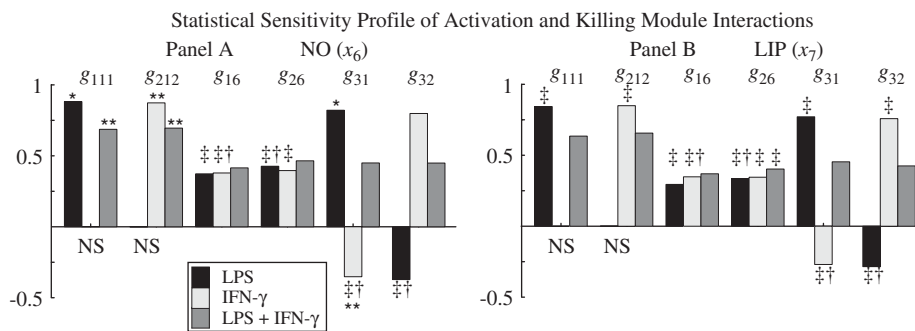


Fig. 4. Significant partial rank correlations (statistical sensitivities) of parameters in activation and killing module interactions to NO levels (x_6) and LIP levels (x_7). Each parameter is shown for three activation states (LPS, IFN- γ and LPS + IFN- γ) at $t = 100$ h. NS: the PRC is not significantly different from zero ($p > 0.01$). Correlations marked ‡ are significantly reduced in absolute value under treatment with exogenous iron ($x_{17} = 10, p < 0.01$). Correlations marked † are not significantly different from zero when a piecewise model is used to prevent suppression of the activation module below the quiescent steady state during partial activation (see text for explanation). *, **: Correlations for the same parameter in the same activation state significantly differ between x_6 and x_7 under both treatment and lack of treatment with exogenous iron (*) or under treatment with exogenous iron only (**). The interaction represented by each parameter is shown in Fig. 1.

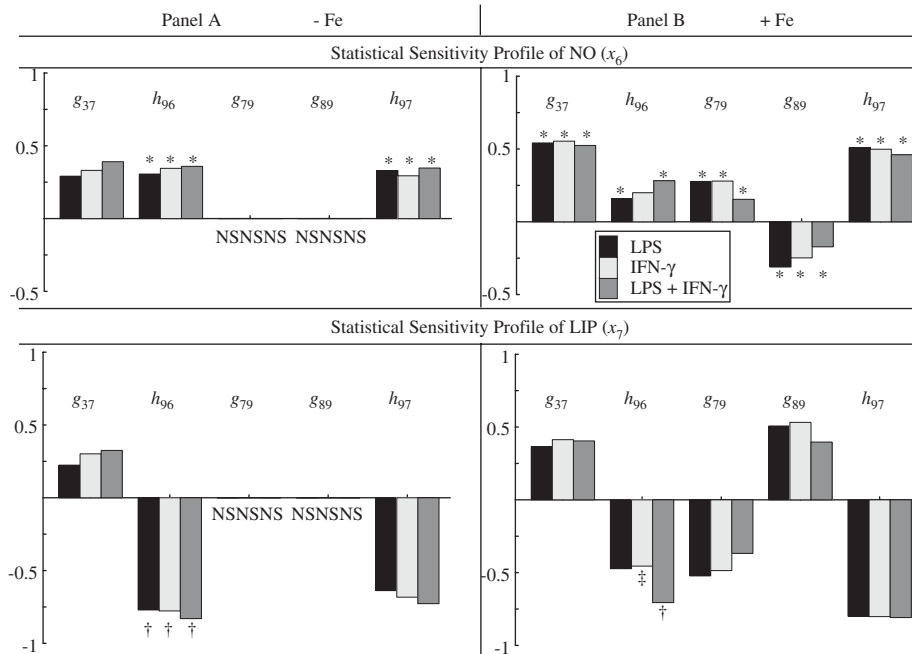


Fig. 5. Significant partial rank correlations (statistical sensitivities) of parameters in the Iron Regulation Module to NO levels (x_6) and LIP levels (x_7). Each parameter is shown for three activation states (LPS, IFN- γ and LPS + IFN- γ) with or without supplemental iron ($x_{17} = 10$) at $t = 100$ h. NS: the PRC is not significantly different from zero ($p > 0.01$). *: Correlations for the same parameter in the same activation state significantly differ between x_6 and x_7 . †: the absolute PRC is significantly greater than $|\gamma_{g_{37},x_6}|$ in the same activation state; ‡: the absolute PRC is significantly less than $|\gamma_{g_{37},x_6}|$ in the same activation state. The interaction represented by each parameter is shown in Fig. 1.

tions with [NO], resulting in the synergistic interaction of the two signals in iNOS/NO production (as in Fig. 3). As the loss of statistical sensitivity of [NO] to some parameters in the piecewise model variant shows (Fig. 4, Panel A †), the crosstalk effect raises the threshold for decisive positive iNOS/NO regulation without the small antagonistic effect seen in the model variant that allows AM suppression. In either case, the PRCs of the transcriptional activation parameters show cooperativity in the two signaling pathways only under full activation signaling.

The statistical sensitivity profile of [LIP] is almost the same as for [NO] for the AM/KM interface parameters due to increased iron uptake under cytokine and endotoxin-induced activation conditions, with significant differences only in g_{111} and g_{31} (Fig. 4; compare PRCs marked * for [NO] (Panel A) with the PRC for the same parameter and activation state for [LIP] in Panel B). Under exogenous iron treatment there are more parameters with significant differences between the sensitivities of [NO] and [LIP] to them (Fig. 4, compare both * and ** in Panel A to the PRC with the same parameter and activation state in Panel B). Furthermore, under exogenous iron treatment the PRC of [LIP] with some interactions is significantly lowered compared to no iron treatment (Fig. 4, Panel B, ‡).

3.2.2. Interactions between the killing and iron regulation modules

We find the statistical sensitivity of [NO] (x_6) to variations in the parameters in the IRM, including those

between the KM and IRM, to be lower than those parameters between the AM and KM (compare Fig. 5 top panels to Fig. 4, Panel A). However, exogenous iron treatment induces a significant change in the PRCs of [NO] for most IRM parameters (Fig. 5, Panel B, top; significance test not shown). The exception is h_{96} , NO-induced regulation of the IRM, in the fully activated state.

Statistical sensitivity of [LIP] (x_7) to IRM parameters is predictably much higher, and generally opposite to [NO] sensitivities (Fig. 5, top * versus bottom). Recall that [LIP] sensitivities to AM/KM parameters mirrored those of [NO]. The best explanation for the reversal in PRCs to IRM parameters between [NO] and [LIP] is that, while an increase in NO production tends to increase iron intake into the LIP, an increase in exogenous iron and resultant [LIP] increase tends to inhibit iNOS transcription and result in a lowering of [NO].

We are therefore interested in which module dominates the immune response under high iron conditions, as [NO] is sensitive to the IRM parameters, and [LIP] is less sensitive to AM/KM parameters under treatment with exogenous iron. By comparing the statistical sensitivity of [NO] to g_{37} (the parameter representing the regulation of iNOS transcription by the LIP), γ_{g_{37},x_6} , to the statistical sensitivity of [LIP] to h_{96} (the parameter representing the regulation of the IRM by NO), γ_{h_{96},x_7} , we can determine which module is dominant under different conditions. For cases without exogenous iron (Fig. 5, Panel A, †) the statistical sensitivity of [LIP] to h_{96}

(bottom) is significantly higher than the statistical sensitivity of [NO] to g_{37} (top) in every activation state. This changes during elevated exogenous iron conditions (Fig. 5, Panel B, † and ‡), when the absolute PRC of [LIP] with h_{96} is either not significantly different, or slightly significantly smaller than the absolute PRC of [NO] to g_{37} in partial activation states. However, under complete activation, we find the absolute PRC of [LIP] with h_{96} to be elevated, restoring the relationship seen under no iron treatment above.

We conclude that with complete activation, the synergistic interaction of LPS and IFN- γ activation pathways overcome the KM inhibition by the IRM even in conditions of elevated iron, leaving only incremental differences in parameter statistical sensitivity. However, under partial activation conditions, the statistical sensitivity of the KM to the IRM is approximately in parity with that of the IRM to the KM.

Table 4
Predicted parameter regions that best meet each criterion denoted by a score of -, 0 or +

Parameter	Stability	Responsiveness	Robustness ^a	Overall score
g_{31}	+	+	≈	Positive
g_{32}	+	+	≈	Positive
g_{16}	-	-	-	Negative
g_{26}	-	-	-	Negative
g_{37}	-	-	≈	Negative
h_{96}	-	-	-	Negative

^aIn some cases for the robustness criterion, there was not a clear score derived from gains and sensitivities (see Fig. 7); however, taken together, the other two criteria suggest a clear overall score. See text for details.

3.3. Local analysis: Evolutionary requirements for inter-module interactions

Each interaction coupling the functional modules may be stimulatory or inhibitory. The types of interactions present determine the functional effectiveness of the macrophage and ensure that the parameter values giving the trade-off between quiescence and strong activation in this model are biologically plausible. For each interaction between the functional modules (Table 2) we have evaluated the model according to three CFE (see Methods), scoring each parameter as stimulatory (+), inhibitory (-) or zero (0) according to the type of interaction that meets the requirements of each criterion (Table 4). We illustrate the evaluation of two parameters, NF- κ B transcription (g_{31}) and NO feedback to NF- κ B (g_{16}) (Figs. 6–8), according to the CFE.

As discussed in Methods, several interactions in the model are idealized and may be stimulatory or inhibitory depending on the predominant mechanism assumed in the model. We consider this plausible for the interactions of nitric oxide with other system components (g_{16} , g_{26} and h_{96}). The transcriptional regulation parameters (g_{31} , g_{32} and g_{37}) have known or postulated mechanisms of either stimulation or inhibition, though they may differ based on cell type (Ganster et al., 2001). Regardless, we examine these three parameters assuming any type of interaction is possible. This allows us to see (i) confirmation that this model predicts the correct interaction type, (ii) how the evolution of positive transcriptional regulation may be favored even in a system with many possible negative side effects (i.e. nitric oxide production), and (iii) how the coupling of iron regulation to NO production affects macrophage activation and iron regulation.

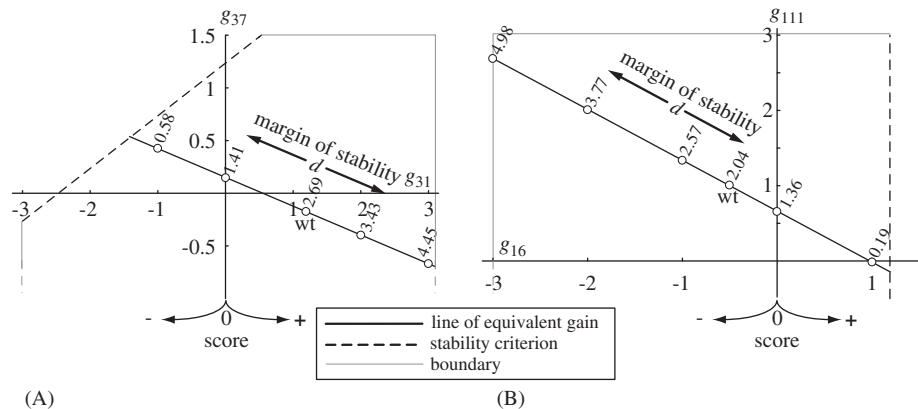


Fig. 6. Each graph shows the parameter space for two of the six controlled comparisons. A single point represents a set of parameter values for the mathematical model. On the x-axis is the knockout parameter (see text). Models meeting the equivalence requirements (Methods; Table 2) are compared along the solid line of equivalence (given in Table 3). This line specifies a value of the parameter on the y-axis that must be chosen to ensure equivalence between versions of the model compared while varying the x-axis parameter. The dashed line represents the Routh–Hurwitz criterion that determines model stability (see Methods). The boundary line represents plausible limits of biological relevance for parameter values. The exact value of each boundary is unknown, but need not be specified for this analysis. The margin of stability d is a measure of distance from a point on the line of equivalent gain to the critical stability line, so that the region with the highest d gives the score for the stability criterion. (A) Parameter space for the transcriptional activation parameter g_{31} . (B) Parameter space for the feedback parameter g_{16} . Points on the line of equivalent gain to the right of the y-axis give a model with a stimulatory interaction represented by the parameter of interest; to the left, the interaction is inhibitory and on the y-axis it is nullified.

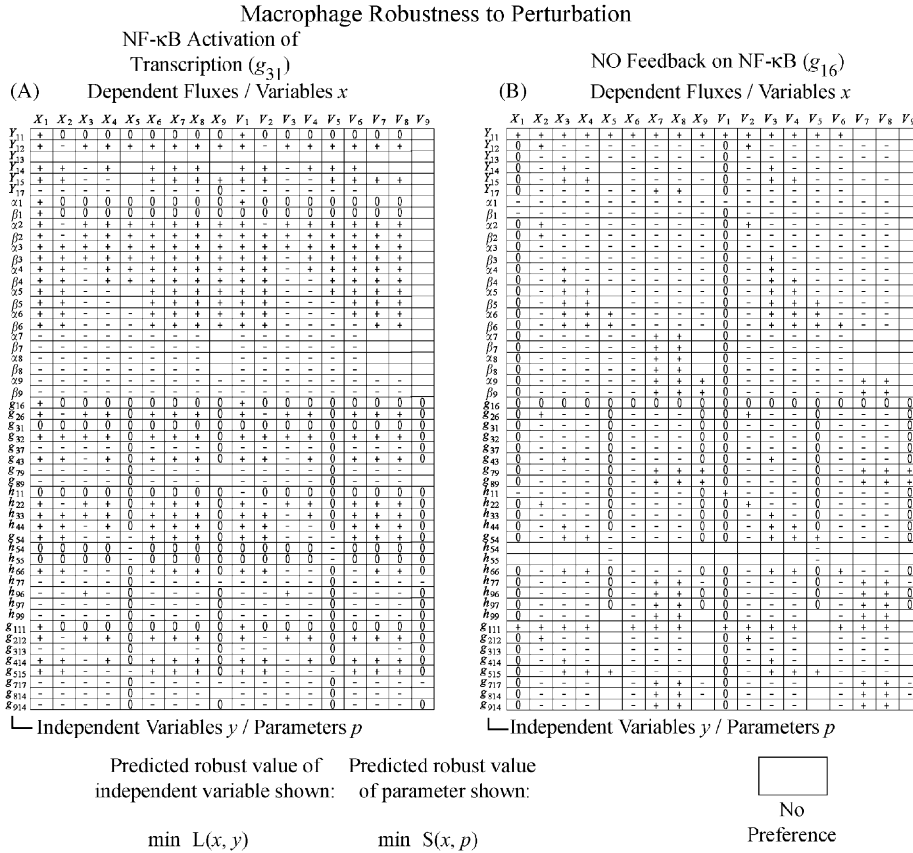


Fig. 7. Scores for g_{31} (panel A) and g_{16} (panel B) that maximize robustness of each dependent flux and variable to perturbation of independent variables $Y_j = \log X_j$ and parameters p during quiescence. Each logarithmic gain $L(X_i, X_j)$ or sensitivity $S(X_i, p)$ is minimal at the score indicated by -, 0, or +. White boxes containing 0 indicate a score of 0 while those with no marking indicate no scoring preference for robustness. Note that the parameter of interest is varied on its line of equivalent gain (Table 3). See Methods for definitions of $L(X_i, X_j)$ and $S(X_i, p)$.

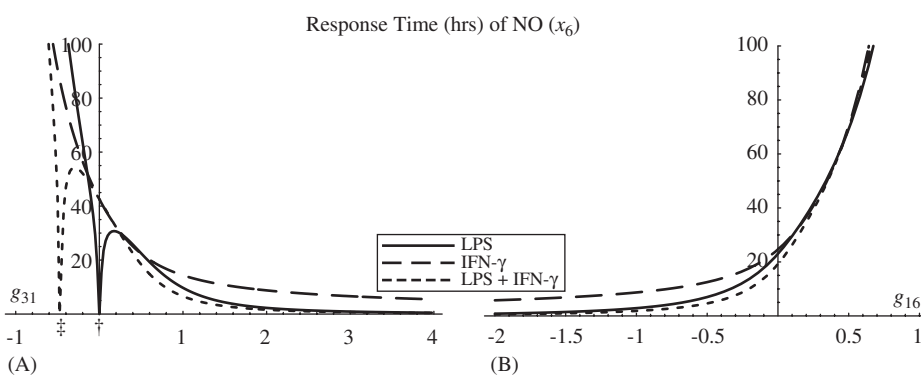


Fig. 8. Response time of nitric oxide (x_6) from quiescent levels to within 5% of the steady state or above for various levels of (A) NF-κB transcriptional regulation (g_{31}) and (B) NO feedback on NF-κB (g_{16}). The knockout parameter of interest is varied along its line of equivalent gain (Table 3). The minimal response time indicates a score of (A) + and (B) -. Depending on the activation state, the profile differs slightly, but a common minimum response parameter value is shared by all activation states in every case. In (A), two of the cases show a trivial minimal response time for $g_{31} = 0$ (marked †) or $g_{31} < 0$ (marked ‡). These cases are irrelevant as the system represented by those parameter values is completely non-responsive to the simulated activation stimuli. No such non-responsive state exists for treatment by IFN- γ alone because of the equivalence requirements imposed on the system (Table 2).

For each criterion, we consider the parameter under investigation to be wild-type if it is at its baseline estimated value (Table 1). We vary the parameter along the line of equivalent gain (LEG) (Table 3) and determine which parameter value score, +, -, or 0, best fits the criterion.

3.3.1. Stability: return to steady state after a small transient perturbation

The first criterion we explore is stability, or the ability of a system to return to steady state after a transient perturbation. The local stability analysis of this system is

a function of several parameters defined by the appropriate Routh–Hurwitz criterion (see Methods). The stability criterion is represented graphically as dashed lines in Fig. 6. Note that as different parameter values from equivalent systems are chosen along the lines of equivalent gain, the margin of stability, defined as d , correspondingly changes. This distance is independent of the macrophage activation state. The score for this criterion for each parameter is given by the type of interaction giving the largest d . Thus, for the parameter g_{31} (Fig. 6A) we have $d(-) < d(0) < d(+)$, giving a score of $+$ for g_{31} in terms of stability. Similarly, for the parameter g_{16} (Fig. 6B) d is maximized for $g_{16} < 0$, giving a score of $-$ (see Table 3, Stability column for the scores of all the tested parameters).

3.3.2. Robustness: Minimal sensitivity of component levels to perturbation

The most functionally effective macrophage is insensitive to small perturbations, or robust. That is, in the absence of decisive activation signals, the macrophage must stay as close to quiescence as possible. We tested system robustness for each parameter of interest by computing the steady state logarithmic gains $L(x_i, x_j)$ and $L(v_i, x_j)$ of the dependent variables x and fluxes v for each independent variable, and the sensitivities $S(x_i, p)$ and $S(v_i, p)$ for each kinetic order p (Fig. 7; see Fig. 1 for the role of each precursor/independent variable in the model). In some situations a gain may preferentially be large, such as the gain of [NO] in the presence of cytokine. However, each gain calculated here is from a single signal at a time, not the multiple-signal situation required for complete activation as in Fig. 2. We therefore assume that gains to individual signals are preferentially low.

For transcriptional regulation parameters g_{31} , g_{32} and g_{37} , a clear plurality or majority of the gains and sensitivities do not support a single score (Fig. 7A shows the profile for g_{31}). For transcriptional activation by second messengers (g_{31} and g_{32}) we find 32.12% support $+$, 32.82% support 0 and 35.05% support $-$. Here perturbation of AM and KM parameters predominantly supports $+$ and perturbation of IRM parameters supports $-$. For iron regulation of transcription (g_{37}) we find 21.27% support $+$, 37.37% support 0 and 41.36% support $-$. In this case perturbation of AM and KM parameters predominantly supports $-$ while perturbation of IRM parameters predominantly supports 0. We do not consider one score to be definitively supported by the robustness criterion in these cases, and rely on the other criteria for the overall score (Table 4).

The interactions of NO with other model components (represented by parameters g_{16} , g_{26} and h_{96}) show clear pluralities or majorities of one score over the others. In each of the cases a negative value is most robust (48.79% of the gains and sensitivities for g_{16} and g_{26} and 52.47% for h_{96}). The remaining gains and sensitivities are split between a score of 0 (31.88% for g_{16} and g_{26} ; 32.58% for h_{96}) and $+$ (19.33% for g_{16} and g_{26} ; 14.94% for h_{96}), leaving—as the favored score. This is shown for g_{16} in Fig. 7B.

3.3.3. Responsiveness: Fast NO elevation after stimulus

A functionally effective system minimizes the time to steady state after stimulus. We explore the response time under which levels of NO (x_6) come within 5% of the activated steady state or above (i.e. we do not penalize the system for overshoot because the goal for killing pathogen should be to get nitric oxide levels up to at least a certain level or above). We examine responsiveness for each of the three activation states with LPS/IFN- γ (Fig. 8). Results with exogenous iron treatment are similar (not shown). As expected, each activation state shows a distinct pattern of response times, but in every case examined, they yield the same score (summarized in Table 4).

The dynamic and specific nature of the numerical simulations leave open several possible situations deserving consideration. If the system starts from a partially activated steady state (i.e. constant stimulus from one signal, say LPS), response times after stimulation from the other signal (here, IFN- γ) are the same as if the system had started in the quiescent steady state. We have also investigated cases with initiation of the two stimulation signals staggered over various short intervals, before the system has reached steady state from the first signal (not shown). The exact profiles differ slightly but in each case the results support the same hypothesis as for other cases. We conclude that examination of the three activation states shown suffice to draw conclusions regarding the responsiveness criterion.

It is possible to achieve a minimal response time representing baseline [NO] that is undisturbed by the activation signal. This is observed for g_{31} (\dagger and \ddagger in Fig. 8A), as well as g_{32} , g_{26} and g_{37} for reasonable parameter ranges. We consider these “non-response” cases to be trivial. Slightly different activation states can change the exact parameter value where this phenomenon occurs. Thus, achieving an artificial minimal response time is likely not relevant since multiple activation signals and the possibility of strong activation are necessary for proper macrophage function. Parameter values less than this no-response point in Fig. 8A represent repressible systems, causing NO levels to decrease in response to stimulus. Determining the response time for g_{16} (Fig. 8B) and h_{96} is more straightforward than the previous cases as levels of NO are induced to a steady state level above that of the quiescent state for biologically reasonable parameter choices.

With the above considerations in mind we conclude that a single score emerges for each parameter examined (Table 4). Therefore g_{31} (Fig. 8A) scores $+$ for responsiveness and g_{16} scores $-$.

4. Discussion

The process of macrophage activation for killing of internalized pathogens has evolved a trade-off between a robustly quiescent state and decisive activation under a definitive signal. Experimental study of this system in

mouse and human cells has characterized components of what are apparently the most important aspects of macrophage activation and killing. This has allowed us to construct a mathematical model for system-level investigation, with a view toward the interaction of functional modules that determine the outcome of activation signaling. Using this model, we have shown that the configuration of intermodule regulatory interactions can permit a near-quiescent state in the presence of partial activation, while allowing complete activation upon receipt of multiple activation stimuli. Our model suggests that there must exist a synergistic response to multiple signals in order to overcome stabilizing interactions for complete macrophage activation. The role of iron regulation in the activation of iNOS and NO production appears to be an asymmetric relationship: iron levels respond to activation as part of the overall response in a pattern consistent with sequestration of iron from extracellular space under normal iron conditions. Mechanisms of killing become sensitive to iron regulation parameters under exogenous iron treatment, but this is most apparent only under partial activation conditions; under complete activation killing mechanisms again predominate.

Each member of an intermodule pair of regulatory interactions (i.e. g_{31}/g_{16} , g_{32}/g_{26} and h_{96}/g_{37}) has a dependence on the other in the pair for the predicted interaction score based on the CFE. Thus, as we know that g_{31} is positive (shown experimentally) then g_{16} is predicted to be negative by the CFE. We also find that anti-inflammatory feedback allows and enforces a system with positive transcriptional regulation as compared to lack of feedback or positive feedback (Figs. 6, 7 and 8B). We therefore see with these interactions how a system that must remain quiescent most of the time can maintain quiescence robustly. This reasoning applies to each of the other pairs of interactions as well. With the KM/IRM interactions (h_{96}/g_{37}) the resultant pair of scores is $-/-$ (Table 4).

AM signaling induces anti-inflammatory feedback to both NF- κ B and Stat1 in this model. The overall effect is to increase the functional effectiveness of the macrophage system (Table 4) by preventing activation in the absence of multiple activating signals. Crosstalk feedback by NO on Stat1 increases the threshold for activation under LPS signaling alone (Figs. 3 and 4). Crosstalk to NF- κ B by IFN- γ signaling also shows this effect to a lesser extent. We explain these results as follows: For transcriptional activation of iNOS, activated NF- κ B, Stat1 and other transcription factors must occupy their promoter regions for transcription initiation and resultant iNOS/NO production. In the absence of an activating signal, the probability of these being together on the promoter is low. When a single activation signal is present (e.g. LPS), the level of NF- κ B increases, raising the probability of transcription initiation. However, the slight increase of NO and resultant negative feedback to Stat1 lowers the probability of Stat1 presence for initiation, or possibly

keeps it at a quiescent level, due to a crosstalk anti-inflammatory feedback effect (Fig. 3). We have shown that this crosstalk-inhibition effect is caused by the negative feedback of NO to the unstimulated activator (Fig. 3). The transcriptional signals are only working in concert under conditions in which both of the signals are sufficiently active. When this is the case the two signals act synergistically to induce NO production (Fig. 2). The activation of multiple signals thus allows the macrophage system to overcome anti-inflammatory feedback for complete activation.

The interactions between the KM and IRM help determine the outcome of LIP levels during activation and the outcome of macrophage activation under iron-rich conditions. The exact effect of macrophage activation on LIP levels may depend on different interactions (Kim and Ponka, 2003; Wang et al., 2005). We find that the most functionally effective motif results in NO production inducing the influx of iron into the LIP via IRPs (i.e. $h_{96} < 0$), increasing LIP levels on the path to sequestration of iron from plasma, consistent with hypoferrremia (Weiss, 2005). Note that one need not argue for a direct benefit of hypoferrremia against extracellular pathogens for this interaction to be functionally effective.

This result shows an indirect negative feedback to iNOS/NO production via the IRM during activation. Under iron-rich conditions this result implies a direct signaling effect of iron influx on iNOS transcription, leading us to question which functional module is dominant. Under a definitive activation signal, the macrophage must show high induction of iNOS and NO in the KM, but this could be inhibited, with potentially impairing results on the immune response, under conditions of high iron in the IRM. We have addressed this with global statistical analysis, which shows a generally higher statistical sensitivity of [LIP] to AM and KM parameters than [NO] shows to IRM parameters under lower level iron conditions. Under iron-rich conditions these statistical sensitivities are brought into near-parity under partial activation conditions (comparing the sensitivity of [NO] to g_{37} to the sensitivity of [LIP] to h_{96} ; Fig. 5), but become asymmetric again under complete activation. Thus exogenous iron appears to play an incremental role in suppressing macrophage activation, particularly important under partial activation conditions. However, this can be overcome so that activation of the KM predominates under complete activation conditions. While the effect of [LIP] on NO production is clear (Weiss et al., 1994; Dlaska and Weiss, 1999; Harhaji et al., 2004), the possible role of this interaction in exacerbating disease processes deserves more study; this model suggests a role for iron in suppressing NO expression by macrophages that depends on the macrophage activation state. This implies that mechanisms required for robust macrophage responses may also worsen response to infection under pathological iron conditions.

Since macrophage activation involves many mechanisms beyond cytokine and endotoxin-induced nitric oxide

production, the scope and applicability of our current work is an important part of thinking about the system. Depending on the mix of cytokines present, macrophages may become activated in a classical or alternative manner (e.g. Gordon, 2003). We have included a subset of mechanisms for classical activation here. Our focus is on quantitative regulation of the model's components; spatial considerations, especially mechanisms of phagocytosis, comprise an important facet of macrophage function that may alter the capability of nitric oxide to access internalized pathogen (e.g. Myers et al., 2003; Miller et al., 2004). Finally, de-activation is a naturally important step in the cycle of macrophage immunological function (reviewed in Gordon, 2003) that has its own set of regulatory apparatus beyond the scope of this model, which is concerned with the process of moving from a quiescent state to activation.

We propose several possible avenues of extension based on our results for the mechanisms of macrophage function presented here. We note first the importance of nitric oxide signaling to transcription factors that regulate iNOS transcription. This may be examined in macrophage culture by detection of nitrosylation crosstalk between signaling pathways. For instance, detecting nitrosylation of Stat1 and other IFN- γ -inducible signals under LPS stimulation (and of NF- κ B and other LPS-inducible signals under IFN- γ stimulation) may further elucidate the roll of NO in activation. Further, the effect of the NO feedback effect may be assessed with consideration for more complex AM interactions not captured here, such as transcriptionally controlled feedback mechanisms. The usefulness of this model may be extended by studying macrophage interactions with a growing population of intracellular bacteria, particularly the superoxide-resistant *Mycobacterium tuberculosis*. Implementation of this extension into the model allows another criterion for macrophage functional effectiveness, namely clearance of bacteria (manuscript in preparation).

Our results show the usefulness of approaching questions regarding the immune response with a view toward the integrated function of the system. We propose that known mechanisms for macrophage activation allow contradictory demands of different contexts to be met with a strong activation signal only in the presence of synergistic activation of multiple signals stabilized by anti-inflammatory feedback from a common output of the signaling cascade. With this in mind other immune signaling cascades may show similar topology and behavior, explaining in part the evolutionary need for multiple signals and complex cytokine networks to overcome robustness to perturbations.

Acknowledgments

The authors thank S.T. Chang for assistance with statistical analysis and M.A. Savageau for critical reading of the manuscript. This work was supported by NIH

Grants LM 009027, HL 072682 and HL 68526 (DEK) and GM 07544-26 (JCJR).

Appendix A

A.1. Model equations

We represent the macrophage network S-system shown in Fig. 1 as a series of differential equations:

$$\frac{dX_1}{dt} = \alpha_1 X_{11}^{g_{111}} X_6^{g_{16}} - \beta_1 X_1^{h_{11}},$$

$$\frac{dX_2}{dt} = \alpha_2 X_{12}^{g_{212}} X_6^{g_{26}} - \beta_2 X_2^{h_{22}},$$

$$\frac{dX_3}{dt} = \alpha_3 X_{13}^{g_{313}} X_1^{g_{31}} X_2^{g_{32}} X_7^{g_{37}} - \beta_3 X_3^{h_{33}},$$

$$\frac{dX_4}{dt} = \alpha_4 X_{14}^{g_{414}} X_3^{g_{43}} - \beta_4 X_4^{h_{44}},$$

$$\frac{dX_5}{dt} = \alpha_5 X_{15}^{g_{515}} X_4^{g_{54}} - \beta_5 X_4^{h_{54}} X_5^{h_{55}},$$

$$\frac{dX_6}{dt} = \beta_5 X_4^{h_{54}} X_5^{h_{55}} - \beta_6 X_6^{h_{66}},$$

$$\frac{dX_7}{dt} = \alpha_7 X_{17}^{g_{717}} X_9^{g_{79}} - \beta_7 X_7^{h_{77}} X_8^{h_{78}},$$

$$\frac{dX_8}{dt} = \alpha_8 X_{14}^{g_{814}} X_9^{g_{89}} - \beta_8 X_7^{h_{87}} X_8^{h_{88}},$$

$$\frac{dX_9}{dt} = \alpha_9 X_{14}^{g_{914}} - \beta_9 X_6^{h_{96}} X_7^{h_{97}} X_9^{h_{99}}.$$

In practice we reduce the number of parameters with basic assumptions about the kinetics as well as non-dimensionalization (see Parameter estimation below). This makes numerical simulations possible and gives the following system:

$$\frac{dx_1}{dt} = a_1(x_{11}^{g_{111}} x_6^{g_{16}} - x_1),$$

$$\frac{dx_2}{dt} = a_2(x_{12}^{g_{212}} x_6^{g_{26}} - x_2),$$

$$\frac{dx_3}{dt} = a_3(x_1^{g_{31}} x_2^{g_{32}} x_7^{g_{37}} - x_3),$$

$$\frac{dx_4}{dt} = a_4(x_3 - x_4),$$

$$\frac{dx_5}{dt} = a_5(x_4 - x_4 x_5),$$

$$\frac{dx_6}{dt} = a_6(x_4 x_5 - x_6),$$

$$\frac{dx_7}{dt} = a_7(x_{17} x_9^{g_{79}} - x_7 x_8),$$

$$\frac{dx_8}{dt} = a_8(x_9^{g_{89}} - x_7x_8),$$

$$\frac{dx_9}{dt} = a_9(1 - x_6^{h_{96}}x_7^{h_{97}}x_9^{h_{99}}).$$

A.2. Alternate representation of activation module

Under partial activation conditions the model predicts one of the transcription factors to be below the quiescent steady state. To address differences between this model and a model where this is not possible we represent the fluxes v_{1p}^+ and v_{2p}^+ in a piecewise manner (Savageau, 2002) in some instances:

$$v_{1p}^+ = \begin{cases} a_1x_{11}^{g_{111}}x_6^{g_{16}}, & x_{11}^{g_{111}}x_6^{g_{16}} \geq 1, \\ a_1, & x_{11}^{g_{111}}x_6^{g_{16}} < 1 \end{cases}$$

$$v_{2p}^+ = \begin{cases} a_2x_{12}^{g_{212}}x_6^{g_{26}}, & x_{12}^{g_{212}}x_6^{g_{26}} \geq 1, \\ a_2, & x_{12}^{g_{212}}x_6^{g_{26}} < 1. \end{cases}$$

We avoided the need for identifying an upper limit by simulating LPS and IFN- γ doses low enough to be below signal saturation.

A.3. Parameter estimation

A.3.1. Rate constants

We have estimated the turnover rates a_i for Eqs. (1)–(4) and (6) from half life data (Nelson et al., 2002; Andrews et al., 2002; Brown et al., 1997; Weiss et al., 1994; Llovera et al., 2001; Ying et al., 2001; Kosaka and Shiga, 1996, respectively).

$a_5 = \beta_6 (X_{60}/X_{50}) = a_6 (X_{60}/X_{50})$ at some operating point. Estimation of the NO:NHA ratio is difficult because actual NO levels are rarely measured in experiments. However, at most levels there is more nitrite than NHA, suggesting that there is more NO than NHA (Bugu et al., 1996; Meyer et al., 1997). We assume this ratio to be 2, giving $a_5 = 2a_6$.

$a_7 = \beta_7 X_{80}$. In erythrocytes the turnover half-life of the LIP is about 1 h (Breuer et al., 1995). Estimates for ferritin mass in macrophages range from 3.55×10^{-4} to 8.5×10^{-3} ng/cell (Mateos et al., 1998; Wesselius et al., 1999; Smith et al., 2003). Given an approximate macrophage cell volume of $4990 \mu\text{m}^3$ (Krombach et al., 1997) and average apoferritin subunit size of 19.1 kDa (Harrison and Arosio, 1996) we estimate $X_{80} \in [3.7 \times 10^{-6}, 8.5 \times 10^{-5}]$ M, giving $a_7 \in [2.58, 61.8] \mu\text{mol}/\text{h}$. We take the mean as the default value. This overestimates the levels of apoferritin, because the variable X_8 is for unbound only. It also underestimates it, because it counts molarity of subunits, not molarity of binding capacity. Nevertheless the sensitivity analysis shows that this will suffice for our analysis.

$a_8 = \beta_8 X_{70}$. Assuming an approximately 2-h half life of ferritin (Kim and Ponka, 2002) and $1 \mu\text{M}$ LIP level

(Kakhlon and Cabantchik, 2002) gives an estimate of $40 \mu\text{mol}/\text{h}$. The LIP level is probably an overestimate but we sufficiently vary the parameter during the uncertainty analysis to account for this.

$a_9 = \alpha_9/X_{90}$. Assuming a 1.8 h half-saturation time for IRP2 during return to steady state after depletion (Kim and Ponka, 2002), and total IRP2 levels in the cell of $0.00874\text{--}0.0132 \mu\text{M}$ (derived from IRP1 numbers (Hentze and Kuhn, 1996) and estimated IRP1/IRP2 ratios (Recalcati et al., 1999)) we estimate $a_9 \in [29.2, 44.1] \text{h}^{-1} \mu\text{M}^{-1}$. We take the mean 36.7 as the default value.

A.3.2. Kinetic orders

General methods for estimation of kinetic orders are found in Voit (2000). Several kinetic order parameters correspond to simple first order processes. When this occurs, the kinetic order is 1. This has been shown experimentally for the following parameters: h_{11} (Nelson et al., 2002), h_{22} (Haspel and Darnell, 1999), h_{33} (Brown et al., 1997), h_{44} (Salimuddin et al., 1999), h_{66} (Thomas et al., 2001) (see below) and h_{99} (Kim et al., 2004). The process of translation is 1-to-1 from mRNA to protein subunit so $g_{43} = 1$. The kinetic orders of iNOS substrate catalysis (g_{54} and h_{54}) are 1 because of the proportionality of iNOS to NO production (Marletta et al., 1988).

We set $h_{55} = 1$, accurate for low levels of NHA. Under high activation conditions, this parameter may be lower (e.g. 0.5 near the $K_m = 15 \mu\text{M}$ (Ghosh et al., 1995)). However, this only affects the steady state of NHA, not any other model components. This would require greater consideration if we were concerned with NHA regulation of arginase (Boucher et al., 1994), but for the aims of this study it suffices to set $h_{55} = 1$.

The kinetic order of NO loss in the intact cellular system $h_{66} = 1$ in hepatocytes (Thomas et al., 2001); the second-order loss often observed in reaction with O_2 is predominant in cell-free systems or extracellular space (e.g. Lewis and Deen, 1994), not relevant here.

Parameters g_{31} , g_{32} , and g_{37} represent transcriptional regulation of the iNOS gene. Based on (McKinney et al. (1998)) we estimate $g_{31} = 1.19$ and $g_{32} = 0.47$ using linear regression of sub-saturation dose response of NO_2^- to LPS and IFN- γ . g_{37} can be estimated to a certain extent by a study showing a 50% decrease in macrophage iNOS mRNA with approximately a 50-fold increase in iron (Weiss et al., 1994) (assuming a $1 \mu\text{M}$ LIP steady state (Kakhlon and Cabantchik, 2002); the estimate does not change significantly even for a substantially lower LIP steady state). Assuming that mRNA stability and other significant components are not altered by the change in iron levels, $g_{37} = \frac{\log 0.5}{\log 50} \approx -0.177$.

The parameters h_{77} , h_{78} , h_{87} , and h_{88} represent the relationship between iron and ferritin and metabolic consumption of the LIP. As discussed in Methods, we represent the ferritin binding capacity instead of the raw number of subunits or complexes. Then one mole of iron takes one mole of ferritin binding capacity and the

parameters of this process (h_{78} , h_{87} , and h_{88}) equal 1. Since X_8 (apoferritin) is an intermediate, its loss due to degradation is negligible. h_{77} represents the weighted average of kinetic orders for loss due to metabolic consumption and chelation by apoferritin. In aggregate, the loss is first order so $h_{77} = 1$ (Breuer et al., 1995).

The parameter g_{89} represents the influence of IRP (X_9) on ferritin (X_8) translation. When IRP2 levels are decreased by the addition of NO^+ , ferritin levels increase linearly over time (Kim and Ponka, 2002). Assuming this assay detected all forms of ferritin, $g_{89} \approx -0.645$.

We set all kinetic orders of independent variables to 1. This has no effect on the model in most cases because the levels of independent variables are arbitrary and usually non-rate limiting. During the course of analysis we choose a value other than 1 for g_{111} and g_{212} for controlled comparisons in some cases (see Local detailed analysis in methods).

The remaining unestimated parameters, h_{96} , h_{97} , g_{79} , g_{16} and g_{26} , represent regulatory interactions for which there exist no quantitative data to our knowledge that would allow us to estimate them. In the default case they are ± 0.5 , equivalent to a Michaelis–Menten process working at the operating point (Voit, 2000).

References

- Alderton, W.K., Cooper, C.E., Knowles, R.G., 2001. Nitric oxide synthases: structure, function and inhibition. *Biochem. J.* 357 (Pt 3), 593–615.
- Andrews, R.P., Ericksen, M.B., Cunningham, C.M., Daines, M.O., Hershey, G.K., 2002. Analysis of the life cycle of Stat6. Continuous cycling of Stat6 is required for IL-4 signaling. *J. Biol. Chem.* 277 (39), 36563–36569.
- Blower, S.M., Dowlatabadi, H., 1994. Sensitivity and uncertainty analysis of complex models of disease transmission: an HIV model, as an example. *Int. Stat. Rev.* 62, 229–243.
- Boucher, J.L., Custot, J., Vadon, S., Delaforge, M., Lepoivre, M., Tenu, J.P., Yapo, A., Mansuy, D., 1994. N^G -hydroxy-L-arginine an intermediate in the L-arginine to nitric oxide pathway, is a strong inhibitor of liver and macrophage arginase. *Biochem. Biophys. Res. Commun.* 203 (3), 1614–1621.
- Breuer, W., Epsztejn, S., Cabantchik, Z.I., 1995. Iron acquired from transferrin by K562 cells is delivered into a cytoplasmic pool of chelatable iron(II). *J. Biol. Chem.* 270 (41), 24209–24215.
- Brown, D.H., Lafuse, W.P., Zwilling, B.S., 1997. Stabilized expression of mRNA is associated with mycobacterial resistance controlled by Nrampl. *Infect. Immun.* 65 (2), 597–603.
- Buga, G.M., Singh, R., Pervin, S., Rogers, N.E., Schmitz, D.A., Jenkinson, C.P., Cederbaum, S.D., Ignarro, L.J., 1996. Arginase activity in endothelial cells: inhibition by N^G -hydroxy-L-arginine during high-output NO production. *Am. J. Physiol.* 271 (5 Pt 2), H1988–H1998.
- Chakravorty, D., Hensel, M., 2003. Inducible nitric oxide synthase and control of intracellular bacterial pathogens. *Microbes. Infect.* 5 (7), 621–627.
- Chauhan, V., Breznan, D., Goegan, P., Nadeau, D., Karthikeyan, S., Brook, J.R., Vincent, R., 2004. Effects of ambient air particles on nitric oxide production in macrophage cell lines. *Cell. Biol. Toxicol.* 20 (4), 221–239.
- Connelly, L., Palacios-Callender, M., Ameixa, C., Moncada, S., Hobbs, A.J., 2001. Biphasic regulation of NF- κ B activity underlies the pro- and anti-inflammatory actions of nitric oxide. *J. Immunol.* 166 (6), 3873–3881.
- Dlaska, M., Weiss, G., 1999. Central role of transcription factor NF-IL6 for cytokine and iron-mediated regulation of murine inducible nitric oxide synthase expression. *J. Immunol.* 162 (10), 6171–6177.
- Ganster, R.W., Taylor, B.S., Shao, L., Geller, D.A., 2001. Complex regulation of human inducible nitric oxide synthase gene transcription by Stat1 and NF- κ B. *Proc. Natl Acad. Sci. USA* 98 (15), 8638–8643.
- Gao, J., Morrison, D.C., Parmely, T.J., Russell, S.W., Murphy, W.J., 1997. An interferon-gamma-activated site (GAS) is necessary for full expression of the mouse iNOS gene in response to interferon-gamma and lipopolysaccharide. *J. Biol. Chem.* 272 (2), 1226–1230.
- Ghosh, D.K., Abu-Soud, H.M., Stuehr, D.J., 1995. Reconstitution of the second step in NO synthesis using the isolated oxygenase and reductase domains of macrophage NO synthase. *Biochemistry* 34 (36), 11316–11320.
- Gordon, S., 2003. Alternative activation of macrophages. *Nat. Rev. Immunol.* 3, 23–35.
- Groves, J.T., Wang, C.C.-Y., 2000. Nitric oxide synthase: models and mechanisms. *Curr. Opin. Chem. Biol.* 4 (6), 687–695.
- Guo, Z., Shao, L., Feng, X., Reid, K., Marderstein, E., Nakao, A., Geller, D.A., 2003. A critical role for C/EBP β binding to the AABS promoter response element in the human iNOS gene. *FASEB J.* 17 (12), 1718–1720.
- Harhaji, L., Vuckovic, O., Miljkovic, D., Stosic-Grujicic, S., Trajkovic, V., 2004. Iron down-regulates macrophage anti-tumour activity by blocking nitric oxide production. *Clin. Exp. Immunol.* 137 (1), 109–116.
- Harrison, P.M., Arosio, P., 1996. The ferritins: molecular properties, iron storage function and cellular regulation. *Biochim. Biophys. Acta* 1275 (3), 161–203.
- Haspel, R.L., Darnell Jr., J.E., 1999. A nuclear protein tyrosine phosphatase is required for the inactivation of Stat1. *Proc. Natl Acad. Sci. USA* 96 (18), 10188–10193.
- Haspel, R.L., Salditt-Georgieff, M., Darnell Jr., J.E., 1996. The rapid inactivation of nuclear tyrosine phosphorylated Stat1 depends upon a protein tyrosine phosphatase. *EMBO J.* 15 (22), 6262–6268.
- Helton, J.C., Davis, F.J., 2000. Sampling-based methods. In: Saltelli, A., Chan, K., Scott, E.M. (Eds.), *Sensitivity Analysis*. Wiley, Chichester, pp. 101–153.
- Hentze, M.W., Kuhn, L.C., 1996. Molecular control of vertebrate iron metabolism: mRNA-based regulatory circuits operated by iron, nitric oxide and oxidative stress. *Proc. Natl Acad. Sci. USA* 93 (16), 8175–8182.
- Herynek, V., Bulte, J.W., Douglas, T., Brooks, R.A., 2000. Dynamic relaxometry: application to iron uptake by ferritin. *J. Biol. Inorg. Chem.* 5 (1), 51–56.
- Hess, D.T., Matsumoto, A., Kim, S.O., Marshall, H.E., Stampler, J.S., 2005. Protein S-nitrosylation: purview and parameters. *Nat. Rev. Mol. Cell. Biol.* 6 (2), 150–166.
- Hlavacek, W.S., Savageau, M.A., 1995. Subunit structure of regulator proteins influences the design of gene circuitry: analysis of perfectly coupled and completely uncoupled circuits. *J. Mol. Biol.* 248 (4), 739–755.
- Howell, D.C., 1987. *Statistical Methods for Psychology*. Duxbury Press, Boston.
- Huang, H., Rose, J.L., Hoyt, D.G., 2004. p38 Mitogen-activated protein kinase mediates synergistic induction of inducible nitric-oxide synthase by lipopolysaccharide and interferon-gamma through signal transducer and activator of transcription 1 Ser727 phosphorylation in murine aortic endothelial cells. *Mol. Pharmacol.* 66 (2), 302–311.
- Irvine, D., 1991. The method of controlled mathematical comparison. In: Voit, E.O. (Ed.), *Canonical Nonlinear Modeling. S-System Approach to Understanding Complexity*. Van Nostrand Reinhold, New York, pp. 90–109.
- Kakhlon, O., Cabantchik, Z.I., 2002. The labile iron pool: characterization, measurement, and participation in cellular processes. *Free Radic. Biol. Med.* 33 (8), 1037–1046.

- Kim, S., Ponka, P., 2002. Nitrogen monoxide-mediated control of ferritin synthesis: implications for macrophage iron homeostasis. *Proc. Natl Acad. Sci. USA* 99 (19), 12214–12219.
- Kim, S., Ponka, P., 2003. Role of nitric oxide in cellular iron metabolism. *Biometals* 16 (1), 125–135.
- Kim, S., Wing, S.S., Ponka, P., 2004. S-nitrosylation of IRP2 regulates its stability via the ubiquitin-proteasome pathway. *Mol. Cell. Biol.* 24 (1), 330–337.
- Konijn, A.M., Glickstein, H., Vaisman, B., Meyron-Holtz, E.G., Slotki, I.N., Cabantchik, Z.I., 1999. The cellular labile iron pool and intracellular ferritin in K562 cells. *Blood* 94 (6), 2128–2134.
- Kosaka, H., Shiga, T., 1996. Detection of nitric oxide by electron spin resonance using hemoglobin. In: Feilisch, M., Stamler, J.S. (Eds.), *Methods in Nitric Oxide Research*. Wiley, New York, p. 373.
- Krombach, F., Munzing, S., Allmeling, A.M., Gerlach, J.T., Behr, J., Dorger, M., 1997. Cell size of alveolar macrophages: an interspecies comparison. *Environ. Health Perspect.* 105 (Suppl. 5), 1261–1263.
- Kwon, S., Newcomb, R.L., George, S.C., 2001. Mechanisms of synergistic cytokine-induced nitric oxide production in human alveolar epithelial cells. *Nitric Oxide* 5 (6), 534–546.
- Lewis, R.S., Deen, W.M., 1994. Kinetics of the reaction of nitric oxide with oxygen in aqueous solutions. *Chem. Res. Toxicol.* 7 (4), 568–574.
- Llovera, M., Pearson, J.D., Moreno, C., Riveros-Moreno, V., 2001. Impaired response to interferon- γ in activated macrophages due to tyrosine nitration of STAT1 by endogenous nitric oxide. *Br. J. Pharmacol.* 132 (2), 419–426.
- Lorsbach, R.B., Murphy, W.J., Lowenstein, C.J., Snyder, S.H., Russell, S.W., 1993. Expression of the nitric oxide synthase gene in mouse macrophages activated for tumor cell killing. Molecular basis for the synergy between interferon- γ and lipopolysaccharide. *J. Biol. Chem.* 268 (3), 1908–1913.
- Marletta, M.A., Yoon, P.S., Iyengar, R., Leaf, C.D., Wishnok, J.S., 1988. Macrophage oxidation of L-arginine to nitrite and nitrate: nitric oxide is an intermediate. *Biochemistry* 27 (24), 8706–8711.
- Marshall, H.E., Stamler, J.S., 2001. Inhibition of NF-kappa B by S-nitrosylation. *Biochemistry* 40 (6), 1688–1693.
- Marshall, H.E., Merchant, K., Stamler, J.S., 2000. Nitrosation and oxidation in the regulation of gene expression. *FASEB J.* 14 (13), 1889–1900.
- Mateos, F., Brock, J.H., Perez-Arellano, J.L., 1998. Iron metabolism in the lower respiratory tract. *Thorax* 53 (7), 594–600.
- McKay, M.D., Conover, W.J., Beckman, R.J., 1979. A comparison of three methods of selecting values of input variables in the analysis of output from a computer code. *Technometrics* 21 (2), 239–245.
- McKinney, L.C., Aquilla, E.M., Coffin, D., Wink, D.A., Vodovotz, Y., 1998. Ionizing radiation potentiates the induction of nitric oxide synthase by IFN- γ and/or LPS in murine macrophage cell lines: role of TNF- α . *J. Leukocyte Biol.* 64 (4), 459–466.
- Meyer, J., Richter, N., Hecker, M., 1997. High-performance liquid chromatographic determination of nitric oxide synthase-related arginine derivatives in vitro and in vivo. *Anal. Biochem.* 247 (1), 11–16.
- Miller, B.H., Fratti, R.A., Poschet, J.F., Timmins, G.S., Master, S.S., Burgos, M., Marletta, M.A., Deretic, V., 2004. Mycobacteria inhibit nitric oxide synthase recruitment to phagosomes during macrophage infection. *Infect. Immun.* 72 (5), 2872–2878.
- Muijsers, R.B., ten Hacken, N.H., Van Ark, I., Folkerts, G., Nijkamp, F.P., Postma, D.S., 2001. L-Arginine is not the limiting factor for nitric oxide synthesis by human alveolar macrophages in vitro. *Eur. Respir. J.* 18 (4), 667–671.
- Myers, J.T., Tsang, A.W., Swanson, J.A., 2003. Localized reactive oxygen and nitrogen intermediates inhibit escape of *Listeria monocytogenes* from vacuoles in activated macrophages. *J. Immunol.* 171 (10), 5447–5453.
- Nathan, C., Shiloh, M.U., 2000. Reactive oxygen and nitrogen intermediates in the relationship between mammalian hosts and microbial pathogens. *Proc. Natl Acad. Sci. USA* 97 (16), 8841–8848.
- Nelson, G., Paraoan, L., Spiller, D.G., Wilde, G.J., Browne, M.A., Djali, P.K., Unitt, J.F., Sullivan, E., Floettmann, E., White, M.R., 2002. Multi-parameter analysis of the kinetics of NF- κ B signalling and transcription in single living cells. *J. Cell. Sci.* 115 (Pt 6), 1137–1148.
- Petrat, F., de Groot, H., Sustmann, R., Rauen, U., 2002. The chelatable iron pool in living cells: a methodically defined quantity. *Biol. Chem.* 383 (3–4), 489–502.
- Recalcati, S., Conte, D., Cairo, G., 1999. Preferential activation of iron regulatory protein-2 in cell lines as a result of higher sensitivity to iron. *Eur. J. Biochem.* 259 (1–2), 304–309.
- Salimuddin, S., Nagasaki, A., Gotoh, T., Isobe, H., Mori, M., 1999. Regulation of the genes for arginase isoforms and related enzymes in mouse macrophages by lipopolysaccharide. *Am. J. Physiol.* 277 (1 Pt 1), E110–E117.
- Savageau, M.A., 1996. Power-law formalism: A canonical nonlinear approach to modeling and analysis. In: Lakshmikantham, V. (Ed.), *World Congress of Nonlinear Analysts 92*, vol. 4. de Gruyter, Berlin.
- Savageau, M.A., 2001. Design principles for elementary gene circuits: Elements, methods, and examples. *Chaos* 11 (1), 142–159.
- Savageau, M.A., 2002. Alternative designs for a genetic switch: analysis of switching times using the piecewise power-law representation. *Math. Biosci.* 180 (1–2), 237–253.
- Schaible, U.E., Kaufmann, S.H., 2004. Iron and microbial infection. *Nat. Rev. Microbiol.* 2 (12), 946–953.
- Smith, J.J., O'Brien-Ladner, A.R., Kaiser, C.R., Wesselius, L.J., 2003. Effects of hypoxia and nitric oxide on ferritin content of alveolar cells. *J. Lab. Clin. Med.* 141 (5), 309–317.
- Theil, E.C., 2003. Ferritin: at the crossroads of iron and oxygen metabolism. *J. Nutr.* 133 (5), 1549S–1553S.
- Thomson, A.M., Rogers, J.T., Leedman, P.J., 1999. Iron-regulatory proteins, iron-responsive elements and ferritin mRNA translation. *Int. J. Biochem. Cell Biol.* 31 (10), 1139–1152.
- Thomas, D.D., Liu, X., Kantrow, S.P., Lancaster Jr., J.R., 2001. The biological lifetime of nitric oxide: implications for the perivascular dynamics of NO and O₂. *Proc. Natl Acad. Sci. USA* 98 (1), 355–360.
- Voit, E.O., 2000. *Computational Analysis of Biochemical Systems: A Practical Guide for Biochemists and Molecular Biologists*. Cambridge University Press, Cambridge, New York.
- Wang, J., Chen, G., Pantopoulos, K., 2005. Nitric oxide inhibits the degradation of IRP2. *Mol. Cell. Biol.* 25 (4), 1347–1353.
- Weiss, G., 2005. Modification of iron regulation by the inflammatory response. *Best Pract. Res. Clin. Haematol.* 18 (2), 183–201.
- Weiss, G., Werner-Felmayer, G., Werner, E.R., Grunewald, K., Wachter, H., Hentze, M.W., 1994. Iron regulates nitric oxide synthase activity by controlling nuclear transcription. *J. Exp. Med.* 180 (3), 969–976.
- Wesselius, L.J., Williams, W.L., Bailey, K., Vamos, S., O'Brien-Ladner, A.R., Wiegmann, T., 1999. Iron uptake promotes hyperoxic injury to alveolar macrophages. *Am. J. Respir. Crit. Care Med.* 159 (1), 100–106.
- Xie, Q.W., Cho, H.J., Calaycay, J., Mumford, R.A., Swiderek, K.M., Lee, T.D., Ding, A., Troso, T., Nathan, C., 1992. Cloning and characterization of inducible nitric oxide synthase from mouse macrophages. *Science* 256 (5054), 225–228.
- Ying, W.Z., Xia, H., Sanders, P.W., 2001. Nitric oxide synthase NOS2 mutation in Dahl/Rapp rats decreases enzyme stability. *Circ. Res.* 89 (4), 317–322.